Atmospheric dynamics II

Atmospheric circulation

Planetary-scale atmospheric circulation

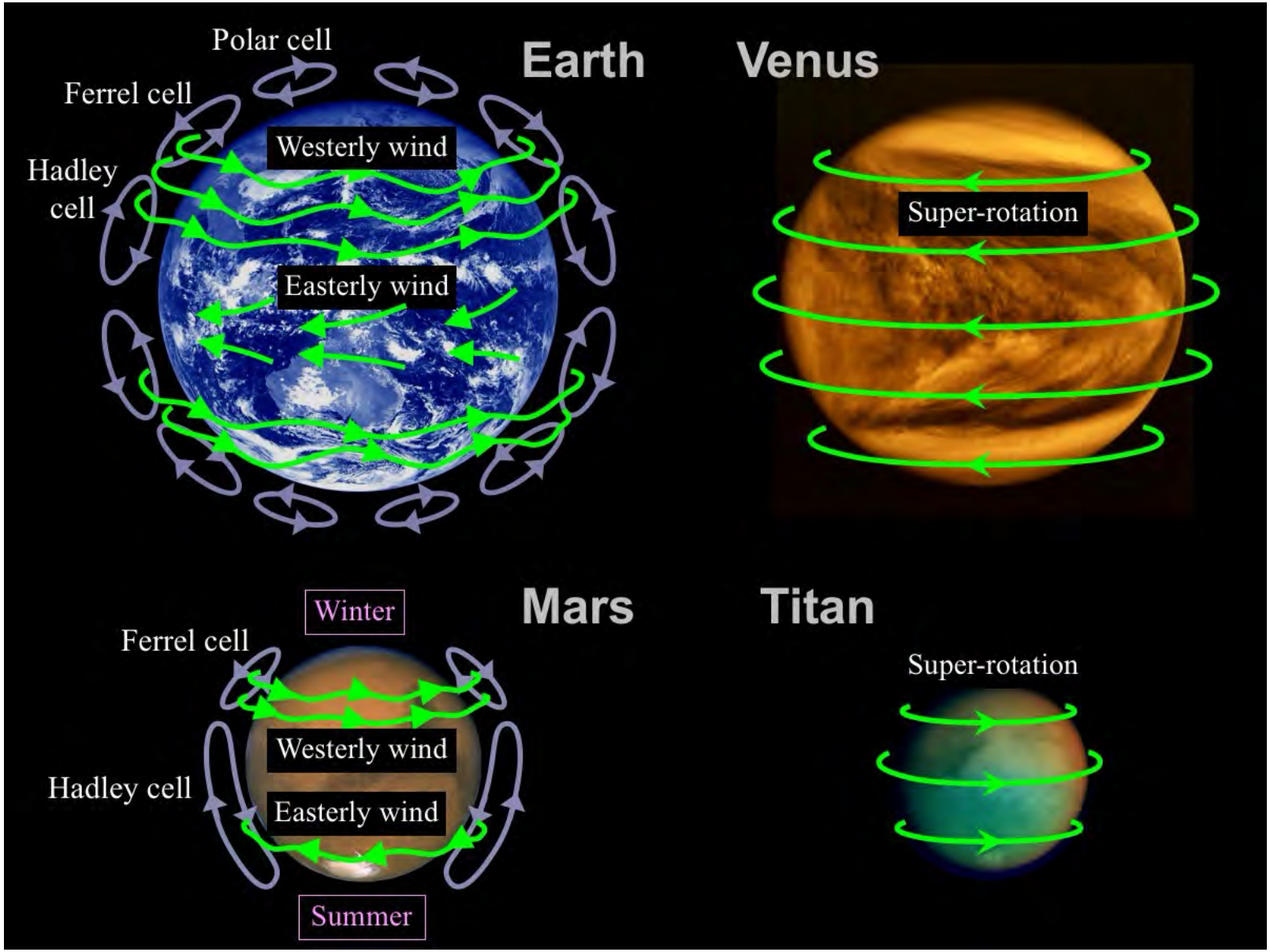

Radiative energy budget and meridional circulation

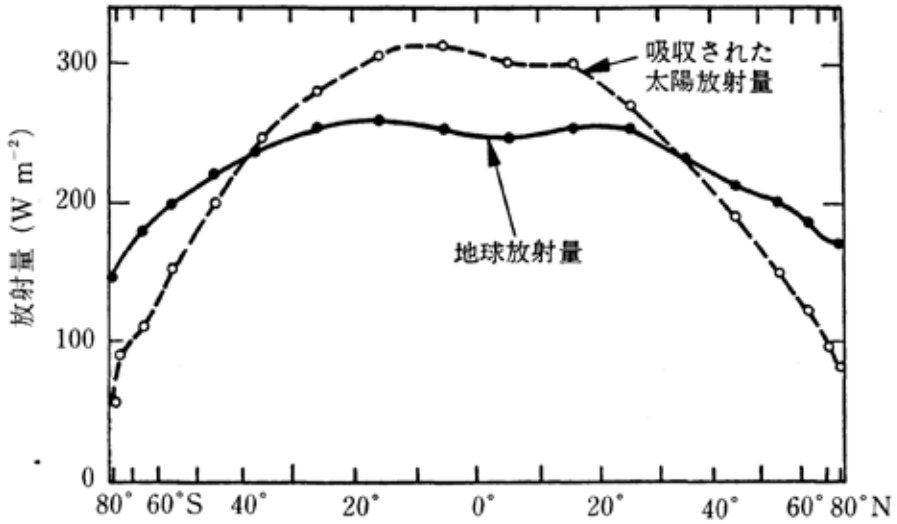

図 4. 4 1962～66 年の衛星観測に基づく帯状平均した放射収支の緯度分布（Vonder Haar and V. Suomi, 1971：*J. Atmos. Sci.*, **28**, 305-314.)

小倉(1978)

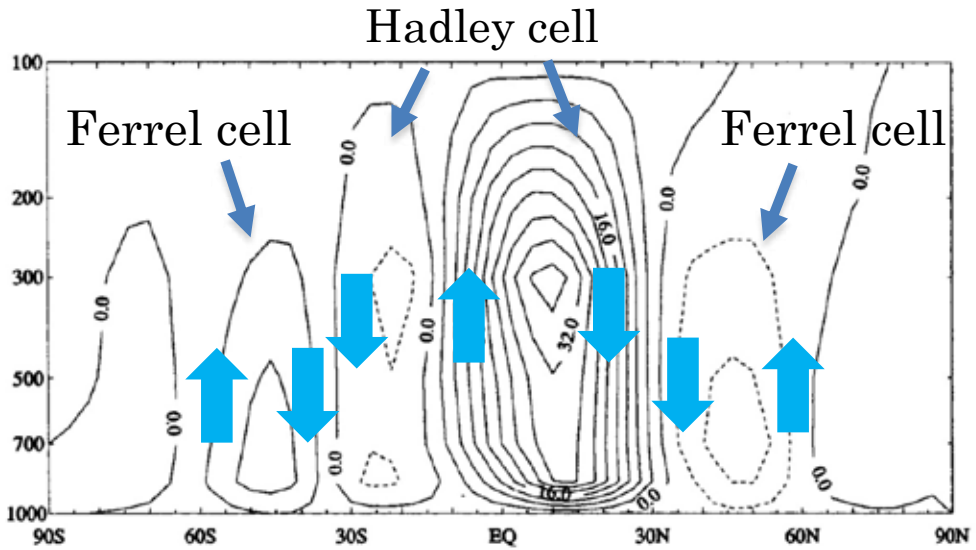

Fig. 10.7 Streamfunction (units: 10^2 kg m^{-1}s^{-1}) for the observed Eulerian mean meridional circulation for Northern Hemisphere winter, based on the data of Schubert et al. (1990).

Holton (2004)

Hadley circulation: a kind of horizontal convection

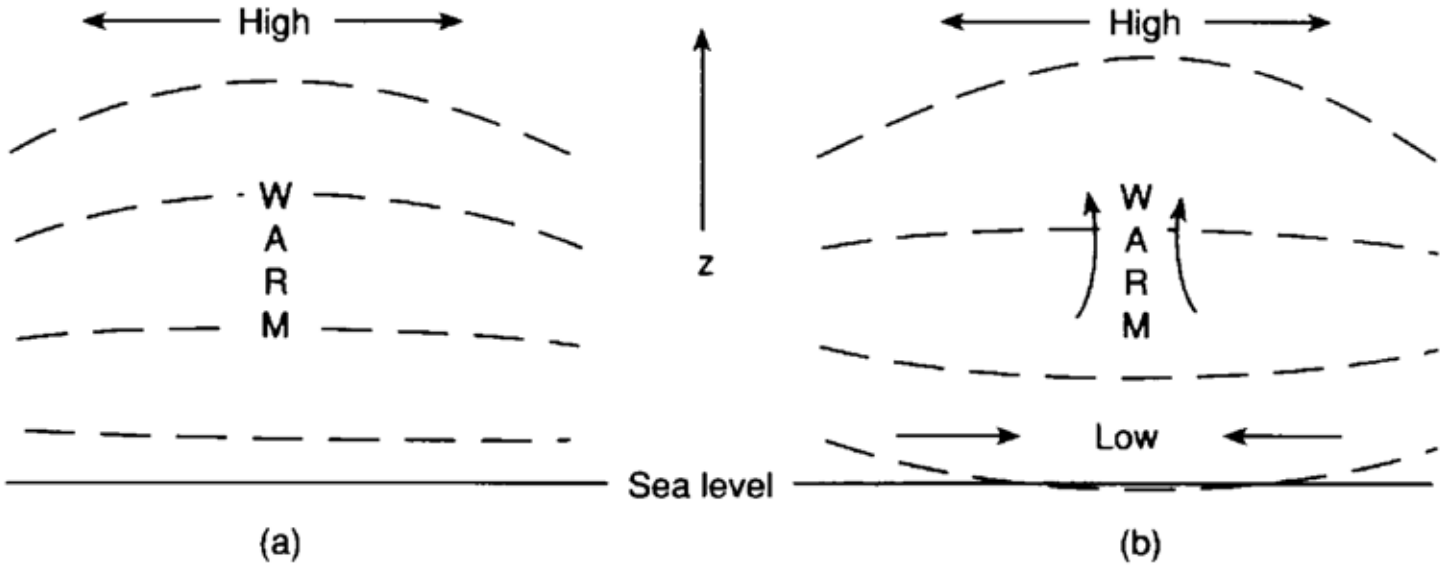

Fig. 3.11 Adjustment of surface pressure to midtropospheric heat source. Dashed lines indicate isobars.

Holton (1992)

Baroclinic wave disturbances

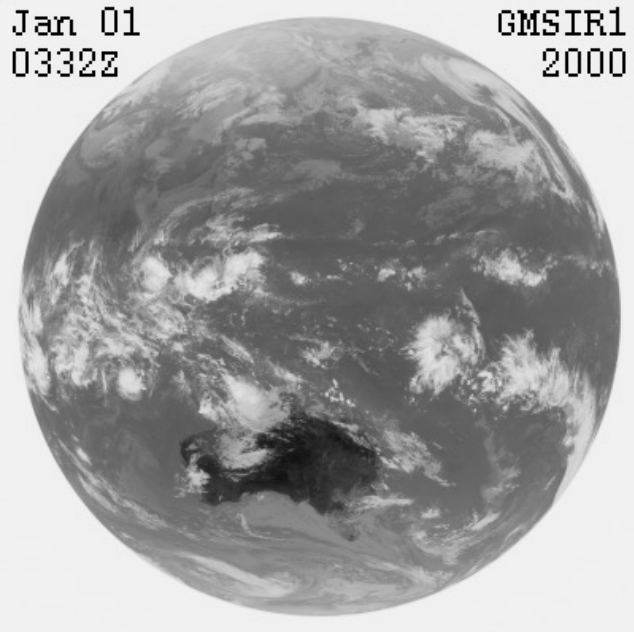

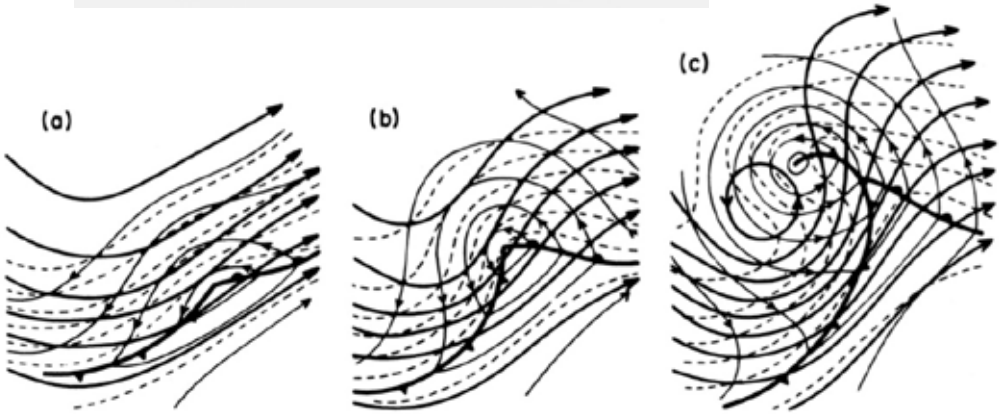

Fig. 6.5 Schematic 500-hPa contours (heavy solid lines), 1000-hPa contours (thin lines), and 1000–500 hPa thickness (dashed) for a developing baroclinic wave at three stages of development. (After Palmén and Newton, 1969.)

Holton 2012

Frontal dust storms on Mars
(Wang et al. 2005)

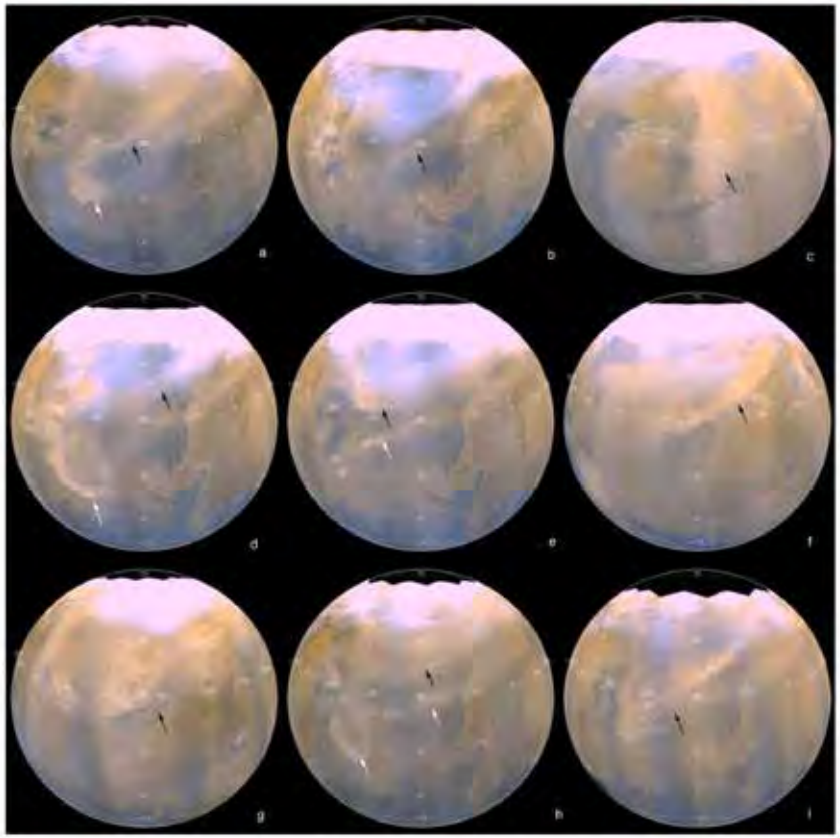

Figure 5. Examples of flushing dust storms in different channels, seasons, and years. Each panel is a Mars daily global map projected onto a sphere with black arrows pointing to the main frontal features. The three rows from the top to the bottom are for MGS mapping Years 1 (1999–2001), 2 (2001–2003), and 3 (2003–2005), respectively. Figures 5a, 5b, 5d, 5e, 5h, and 5i are for the Acidalia channel. Figure 5c is for the Arcadia channel. Figures 5f and 5g are for the Utopia channel. The *Ls* values are (a) 210°, (b) 314°, (c) 336°, (d) 316°, (e) 324°, (f) 324°, (g) 207°, (h) 214°, and (i) 230°.

Quasi-geostrophic vorticity equation

$$\frac{\partial \zeta_g}{\partial t} = -\vec{v}_g \cdot \nabla(\zeta_g + f) + f_0 \frac{\partial \omega}{\partial p}$$

∇ : horizontal differentiation

$\zeta_g \equiv \frac{\partial v_g}{\partial x} - \frac{\partial u_g}{\partial y} = \frac{\nabla^2 \Phi'}{f_0}$: geostrophic vorticity

$\vec{v}_g \equiv \frac{1}{f_0} \vec{k} \times \nabla \Phi$: geostrophic wind

Φ : geopotential

f : Coriolis parameter (planetary vorticity)

$\omega \equiv dp/dt$: vertical velocity in pressure coordinate

Equation of thermodynamics

$$\left(\frac{\partial}{\partial t}+\vec{v}_g\cdot\nabla\right)\frac{\partial\Phi'}{\partial p}+\sigma\omega=0$$

$$\Phi(x,y,p,t)=\overline{\Phi}(p)+\Phi'(x,y,p,t) \quad : \text{geopotential}$$

$$\sigma\equiv-\frac{1}{\overline{\rho}\overline{\theta}}\frac{\partial\overline{\theta}}{\partial p}=\frac{1}{p}\frac{d}{dp}\left(p\frac{d\overline{\Phi}}{dp}-\frac{R}{c_p}\overline{\Phi}\right) \quad : \text{(static stability)}$$

$$\partial\overline{\Phi}/\partial p=-R\overline{T}/p \quad : \text{(temperature)}$$

$$\partial\Phi'/\partial p=-RT'/p \quad : \text{(temperature)}$$

Omega equation

Combining the vorticity equation and the thermodynamics equation to eliminate the time derivative term, we get the “omega equation”:

$$\underbrace{\left(\nabla^2 + \frac{f_0^2}{\sigma}\frac{\partial^2}{\partial p^2}\right)\omega}_{\text{(A)}} = \frac{f_0}{\sigma}\frac{\partial}{\partial p}\left[\vec{v}_g \cdot \nabla(\zeta_g + f)\right] + \frac{f_0 R}{\sigma p}\left[\nabla^2(\vec{v}_g \cdot \nabla T)\right]$$

Let us consider a sinusoidal perturbation

$$\omega \propto \sin(\pi\, p/p_s)\sin(kx)\cos(ly)$$

Then the term (A) becomes

$$\left(\nabla^2 + \frac{f_0^2}{\sigma}\frac{\partial^2}{\partial p^2}\right)\omega \approx -\left[k^2 + l^2 + \frac{1}{\sigma}\left(\frac{f_0\pi}{p_0}\right)^2\right]\omega$$

Since the sign of the vertical velocity *w* is opposite to that of ω ($w \approx -\omega$), (A) is proportional to the vertical velocity. (Upward motion is forced where the right-hand side is positive and downward motion is forced where it is negative.)

Vertical motion forced by the advection of vorticity

Omega equation

$$\underbrace{\left(\nabla^2 + \frac{f_0^2}{\sigma}\frac{\partial^2}{\partial p^2}\right)\omega}_{\approx w} = \underbrace{\frac{f_0}{\sigma}\frac{\partial}{\partial p}\left[\vec{v}_g \cdot \nabla(\zeta_g + f)\right]}_{\text{(B)}} + \frac{f_0 R}{\sigma p}\left[\nabla^2(\vec{v}_g \cdot \nabla T)\right]$$

The term (B) is rewritten as

$$\text{(B)} \propto \frac{\partial}{\partial z}\left(-\vec{v}_g \cdot \nabla\zeta_g - v_g\frac{\partial f}{\partial y}\right)$$

relative vorticity advection

For a short- wave system where relative vorticity advection is larger than the planetary vorticity advection, the pattern of vertical motion forced by the advection of vorticity by the thermal wind has

$w < 0$: west of trough

$w > 0$: east of trough

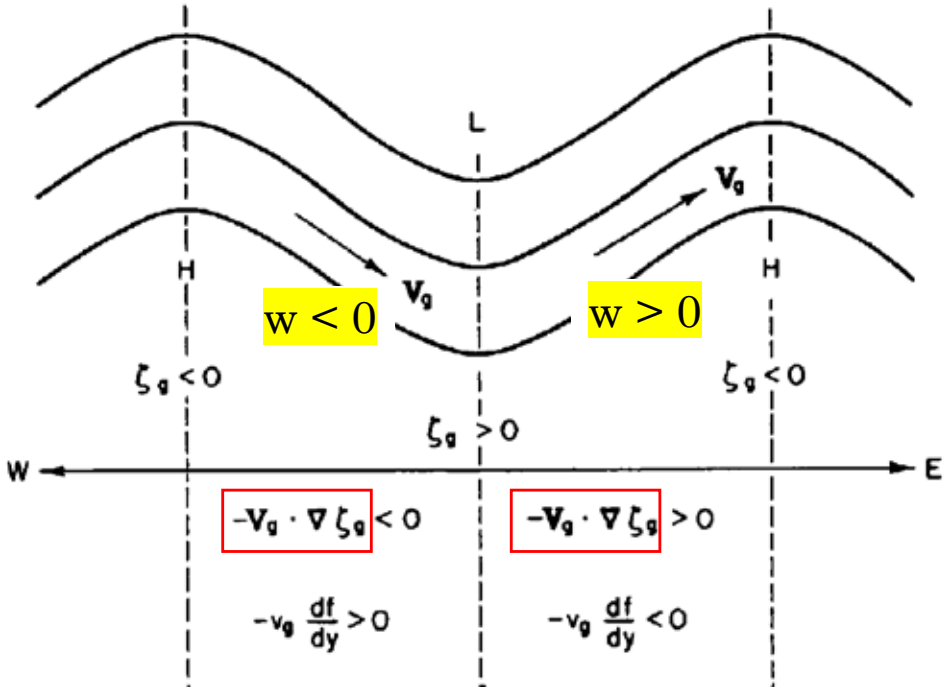

Holton 2004

Eady stability problem for baroclinic disturbances

The structures of unstable modes in a simplified atmosphere with a north-south temperature gradient

- f -plane (β = 0).
- ∂U/∂z = constant.
- Rigid lids at z = 0 and H

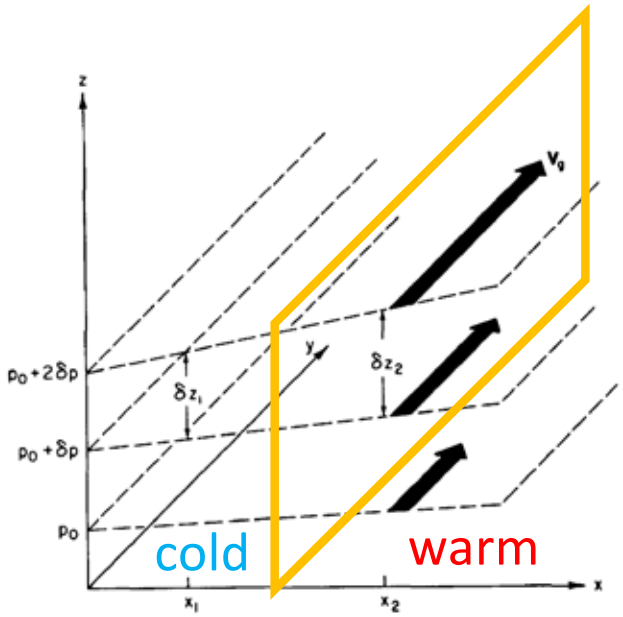

Fig. 3.8 Relationship between vertical shear of the geostrophic wind and horizontal temperature gradients. (Note: $\delta p < 0$.)

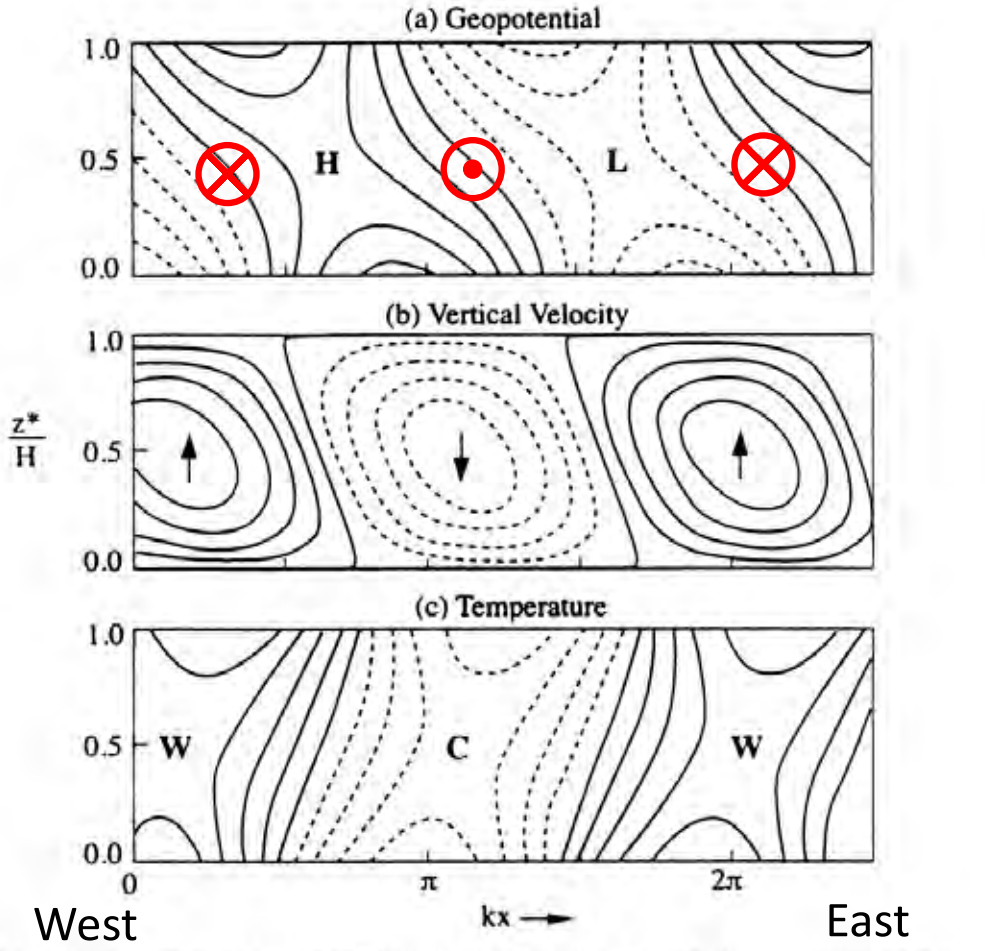

ig. 8.10 Properties of the most unstable Eady wave. (a) Contours of perturbation geopotential height; *H* and *L* designate ridge and trough axes, respectively. (b) Contours of vertical velocity; up and down arrows designate axes of maximum upward and downward motion, respectively. (c) Contours of perturbation temperature; W and C designate axes of warmest and coldest temperatures, respectively. In all panels 1 and 1/4 wavelengths are shown for clarity.

Holton (2004)

3D structure of baroclinic wave disturbance (→ Ferrel cell)

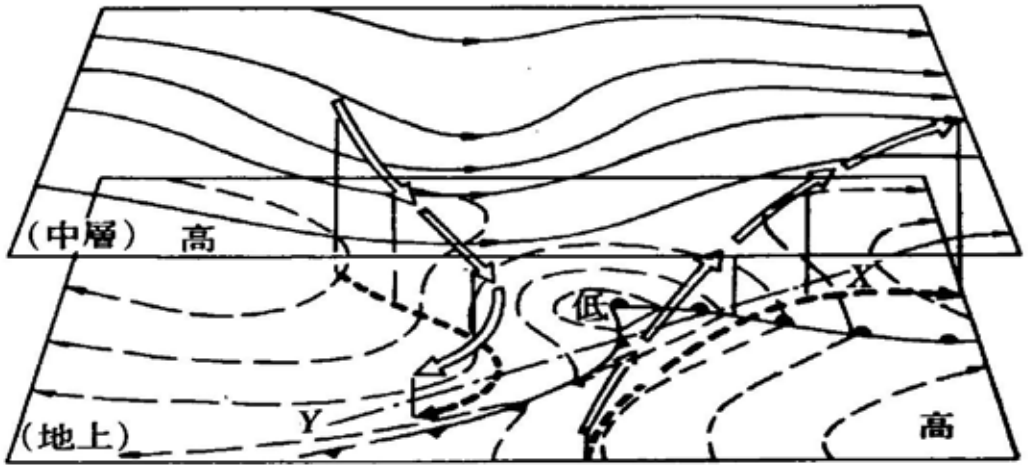

（伊藤 1976）

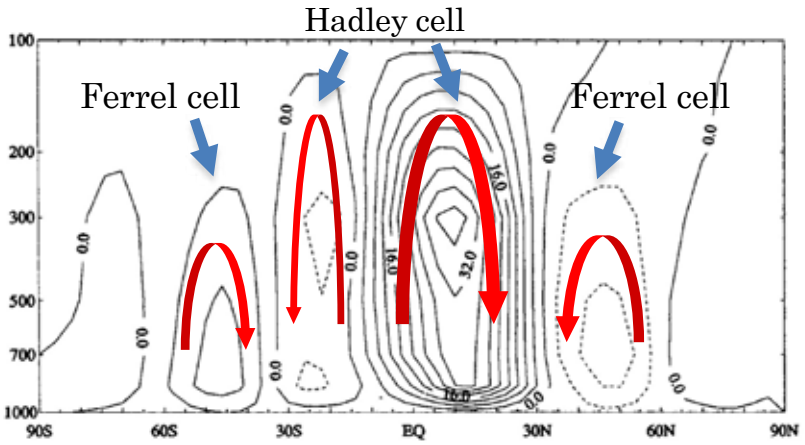

Fig. 10.7 Streamfunction (units: 10^2 kg m^{-1}s^{-1}) for the observed Eulerian mean meridional circulation for Northern Hemisphere winter, based on the data of Schubert et al. (1990).

rising warm air to the east of trough & subsidence of cold air to the west of trough
→ conversion from eddy potential energy to eddy kinetic energy

cold advection below trough → development of trough
warm advection below ridge → development of ridge

Surface meteorological measurements on Mars by Viking-2

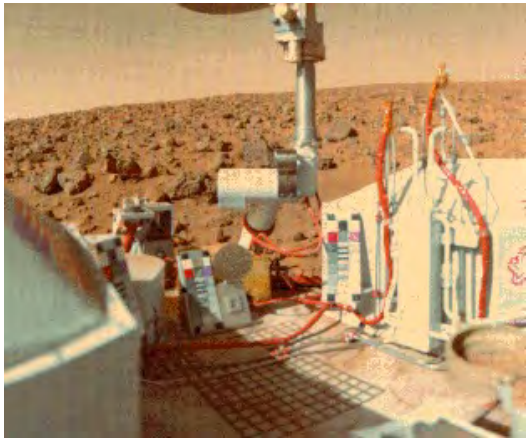

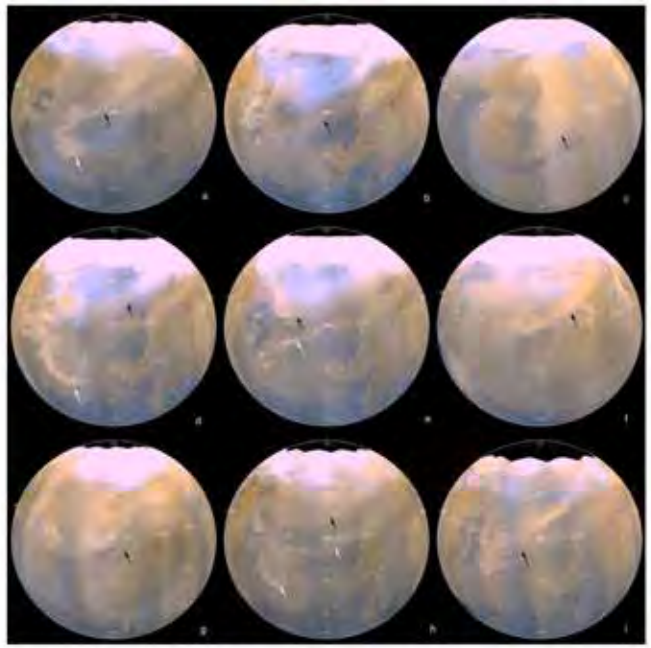

Figure 5. Examples of flushing dust storms in different channels, seasons, and years. Each panel is a Mars daily global map projected onto a sphere with black arrows pointing to the main frontal features. The three rows from the top to the bottom are for MGS mapping Years 1 (1999–2001), 2 (2001–2003), and 3 (2003–2005), respectively. Figures 5a, 5b, 5d, 5e, 5h, and 5i are for the Acidalia channel. Figure 5c is for the Arcadia channel. Figures 5f and 5g are for the Utopia channel. The L_S values are (a) 210°, (b) 314°, (c) 336°, (d) 316°, (e) 324°, (f) 324°, (g) 207°, (h) 214°, and (i) 230°.

(Wang et al. 2005)

(Barnes, 1980)

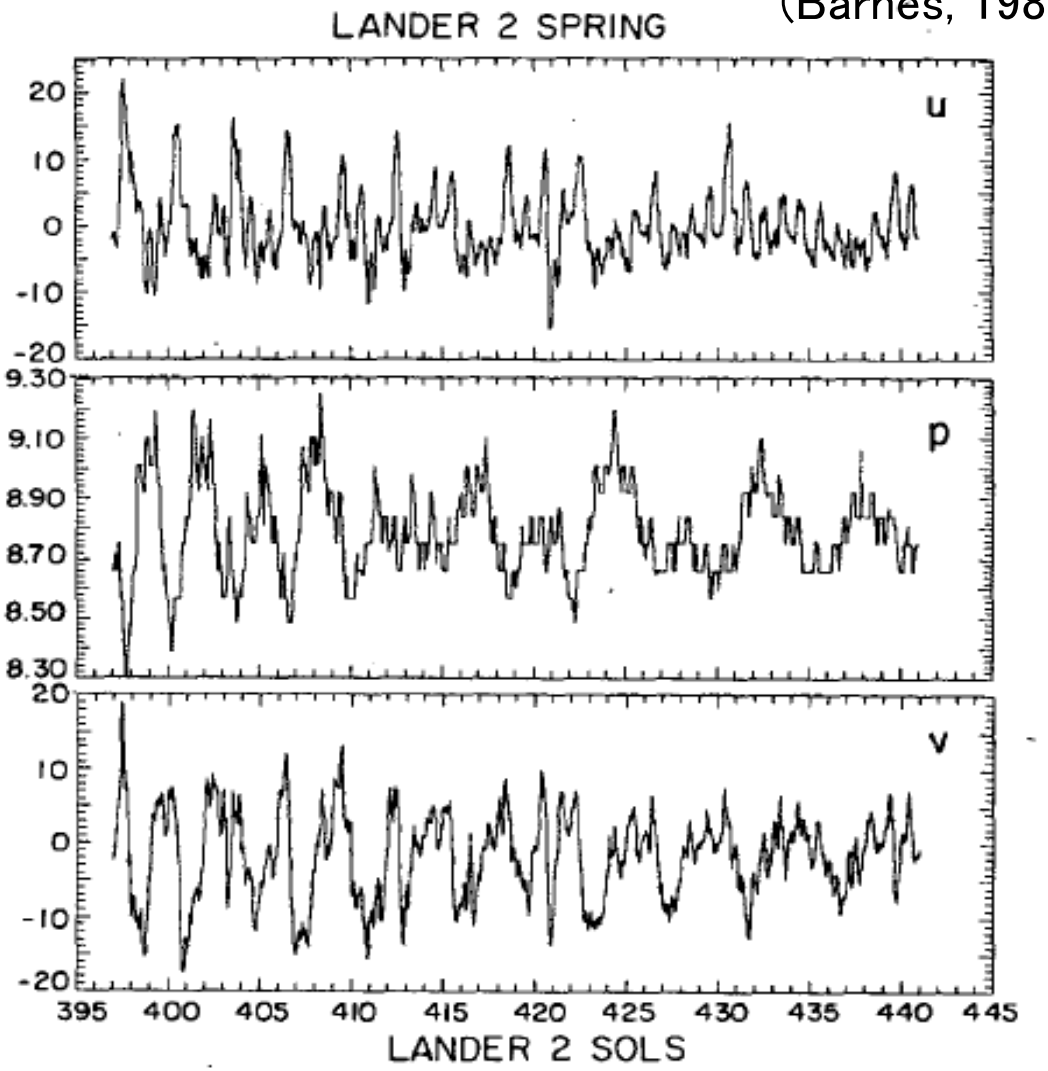

FIG. 2. The unfiltered pressure and zonal (u) and meridional (v) wind data for a 44-sol portion of the spring period at Lander 2. The pressure is in mb, with the wind speeds in m s^{-1}.

Meridional heat transport

$\overline{v'T'}$

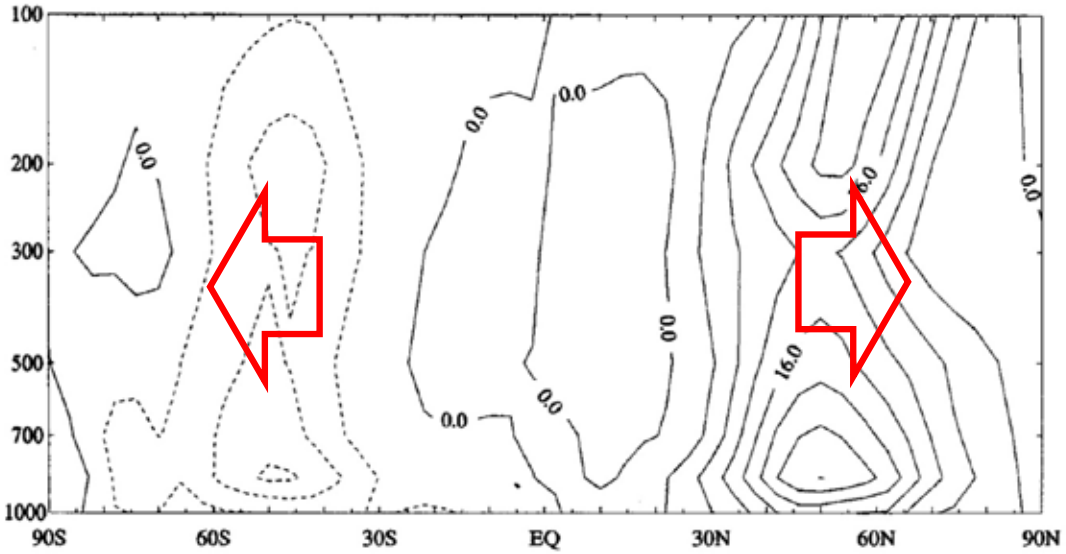

Fig. 10.3 Observed northward eddy heat flux distribution (°C m s^{-1}) for Northern Hemisphere winter. (Adapted from Schubert et al., 1990.)

stream function

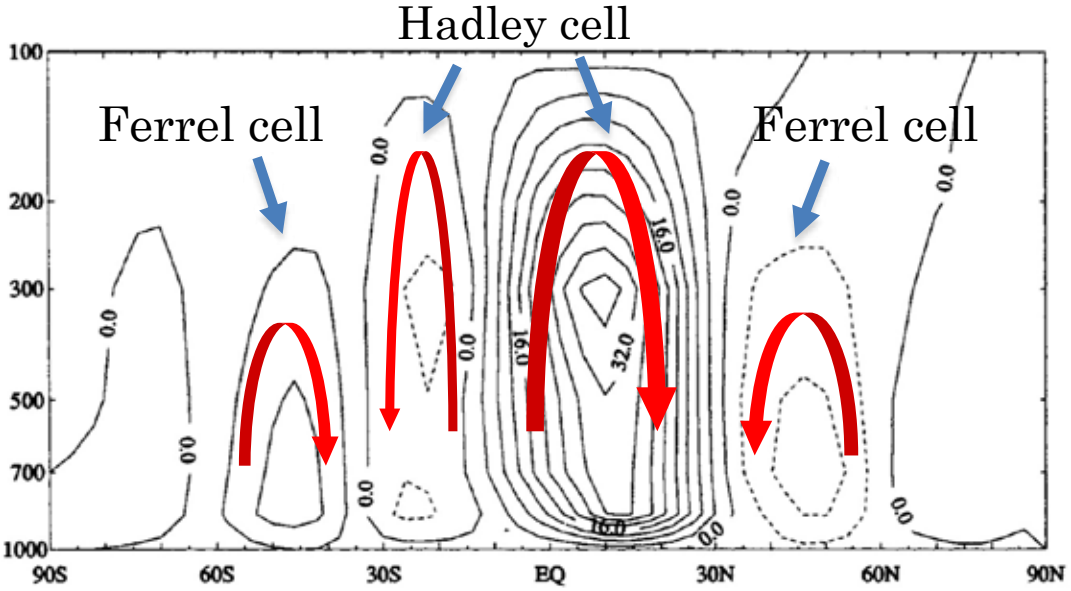

Fig. 10.7 Streamfunction (units: 10^2 kg m^{-1}s^{-1}) for the observed Eulerian mean meridional circulation for Northern Hemisphere winter, based on the data of Schubert et al. (1990).

Holton 2004

Meridional circulation in a Martian GCM (general circulation model)

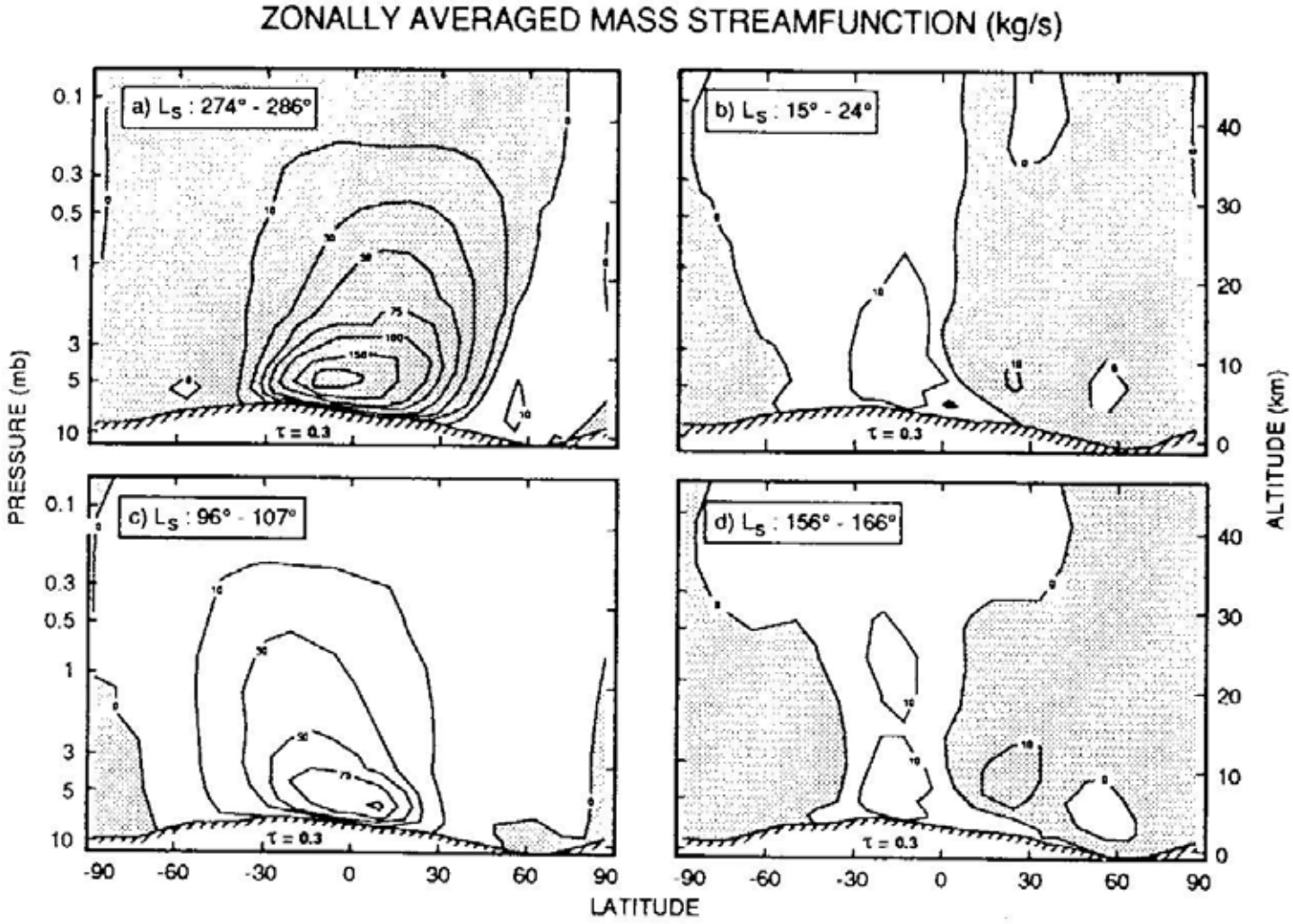

Fig. 19. Mass-weighted stream functions computed by the Mars-GCM (Pollack et al. 1990*a*) for early northern winter (a: $L_s \approx 280°$), early northern spring (b: $L_s \approx 20°$), early northern summer (c: $L_s \approx 103°$) and late northern summer (d: $L_s \approx 161°$). A background dust opacity of $\tau = 0.3$ was assumed. Flow in the meridional plane is clockwise around minima (negative values are shaded) and anti-clockwise around maxima; winds are strongest where contours are closest.

(Pollack et al 1990)

Baroclinic instability in Venusian atmosphere?

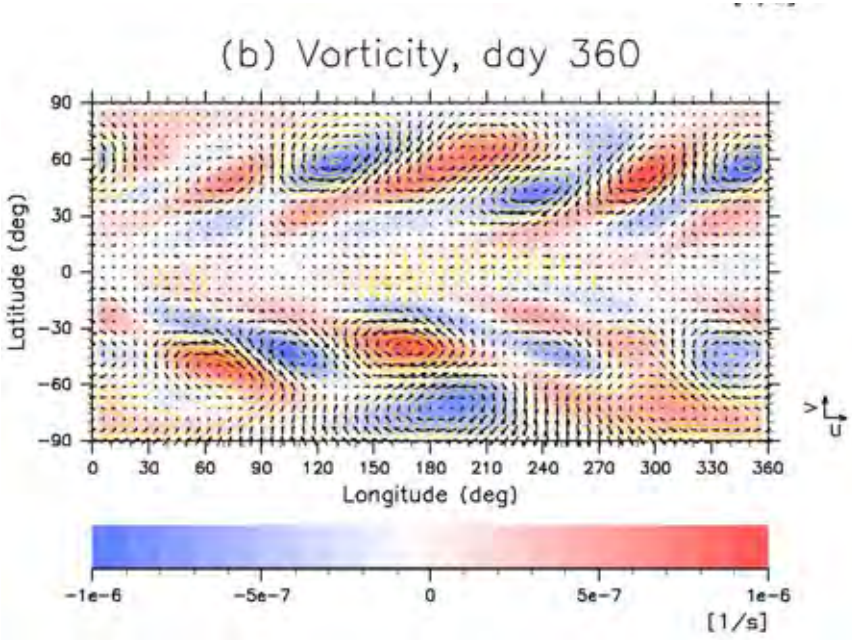

Sugimoto et al. (2014)

The superrotation of the atmosphere takes the place of planetary rotation, thereby sustaining baroclinic instability

2.26 μm image of Venusian nightside taken by Akatsuki IR2

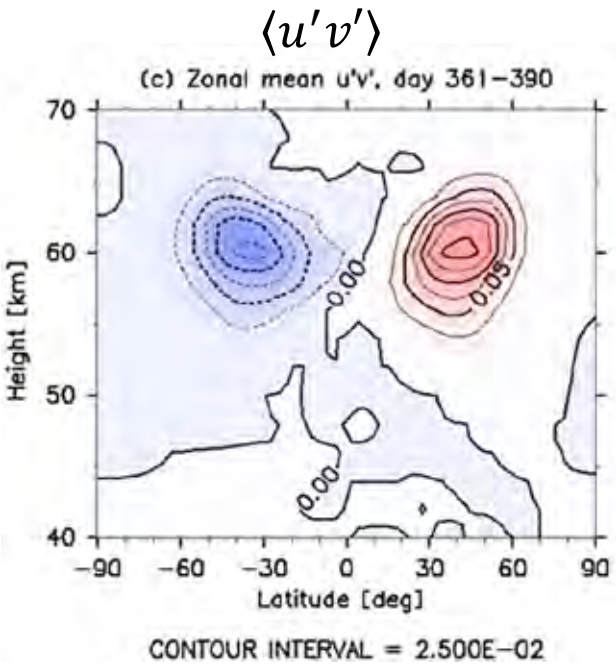

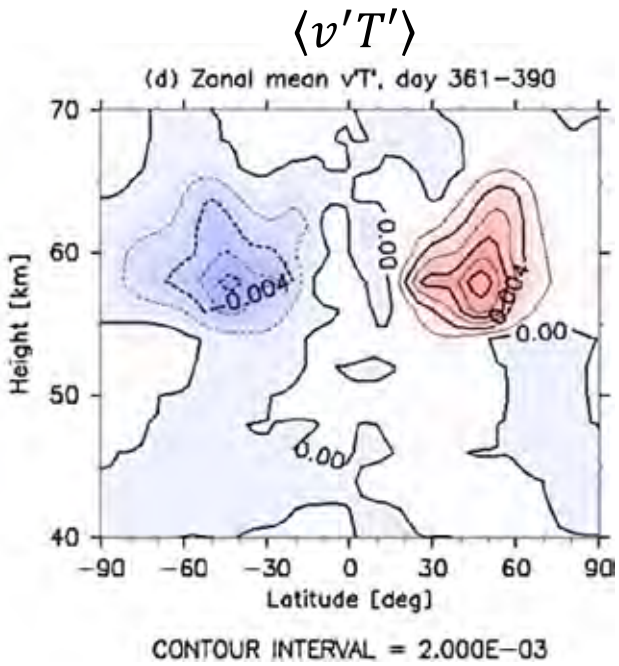

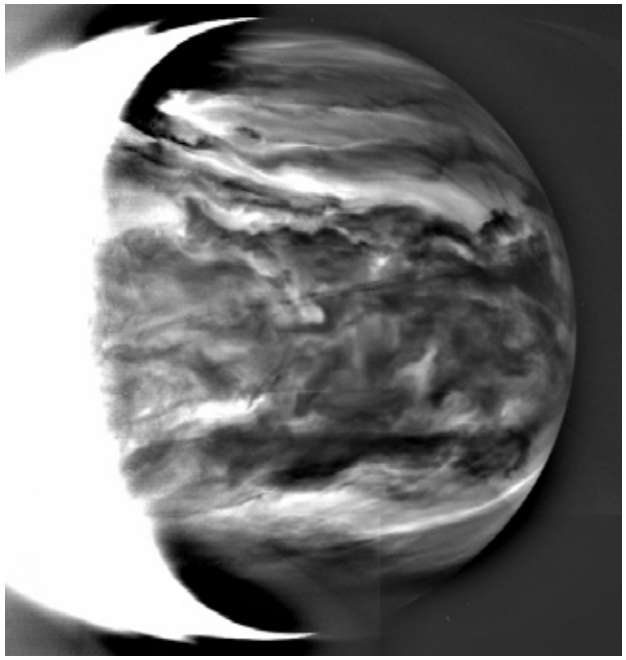

wave momentum transport

baroclinic instability

→ generation of Rossby waves

→Rossby waves take away retrograde (westward) angular momentum from the md-latitude

→ maintenance of (eastward) mid-latitude jets

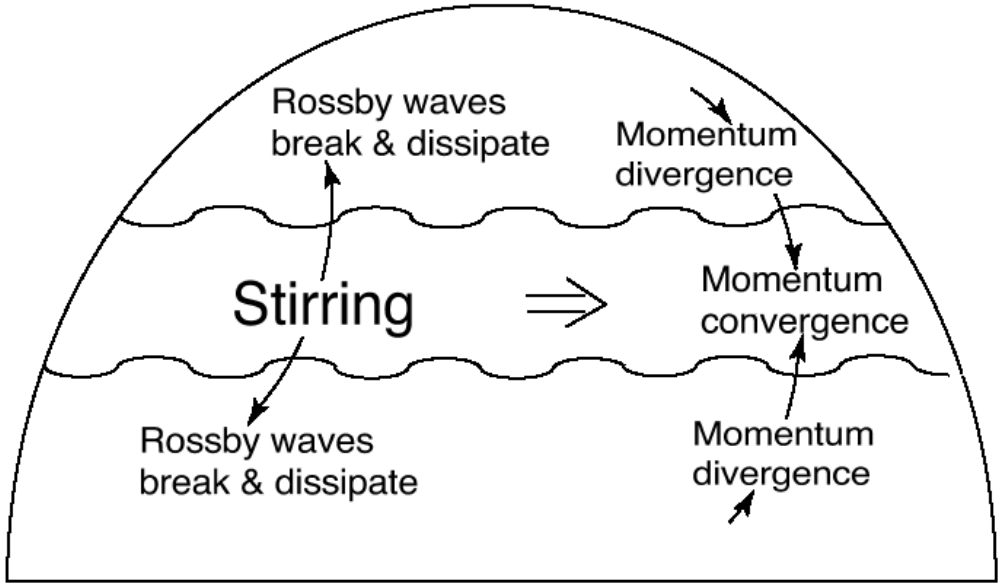

(Vallis, 2005)

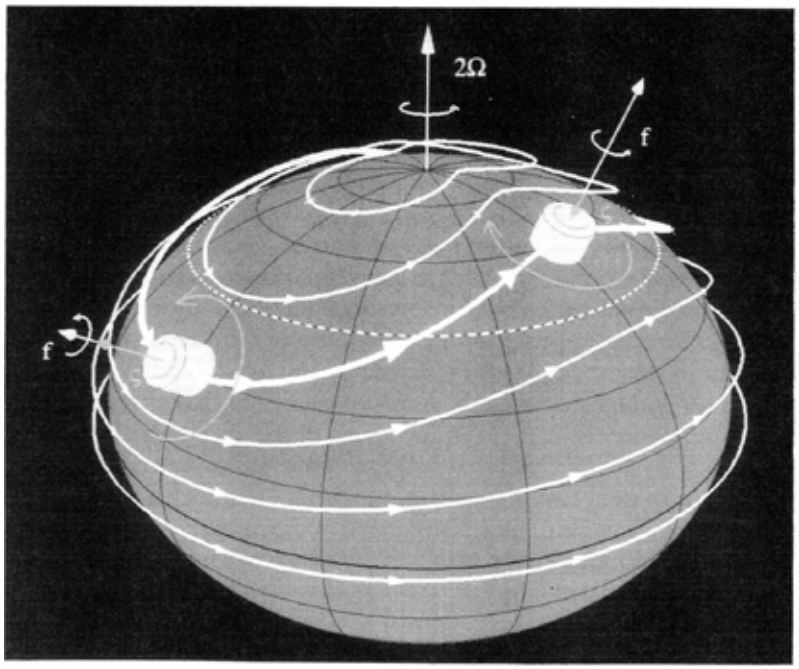

(Salby, 1996)

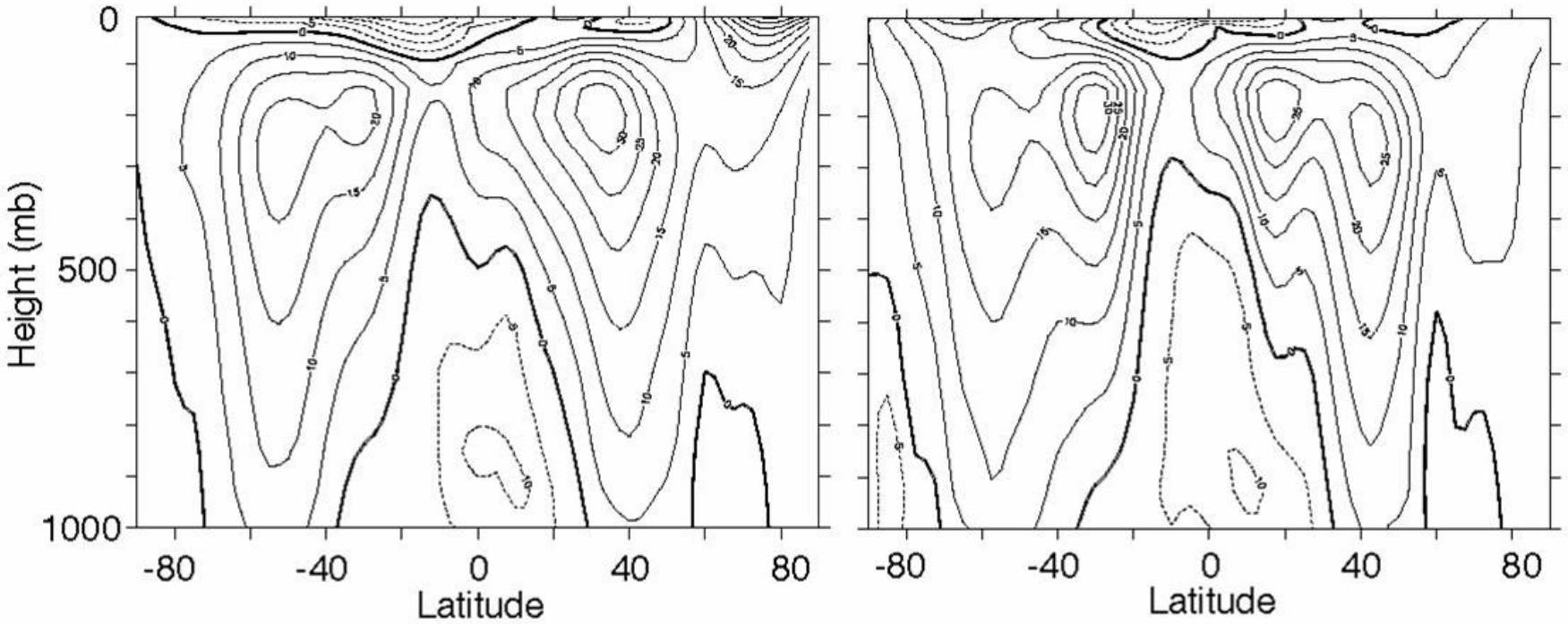

Fig. 3.1 The time-averaged zonal wind at 150°W (in the mid Pacific) in December-January February (DFJ, left), March-April-May (MAM, right). The contour interval is 5 m s^{-1}. Note the double jet in each hemisphere, one in the subtropics and one in midlatitudes. The subtropical jets is associated with strong meridional temperature gradient, whereas the midlatitude jets have a stronger barotropic component and are associated with westerly winds at the surface.

Vallis (2006)

Latitudinal structures

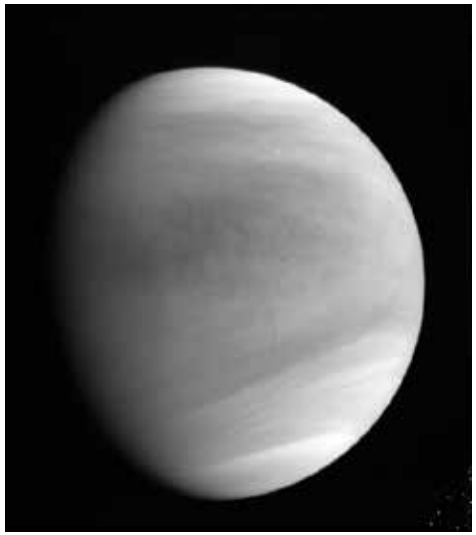

Rotation period	243 days	1 day	10 hours

Rossby radius of deformation

$$L_R = \frac{\sqrt{gH}}{f}$$

g : gravitational acceleration
H : depth of the system
$f = 2\Omega \cos\theta$: Coriolis parameter

The characteristic scale at which the velocity field and the pressure field adjust with each other to maintain geostrophic flow

Faster planetary rotation leads to large f, and then shorter L_R

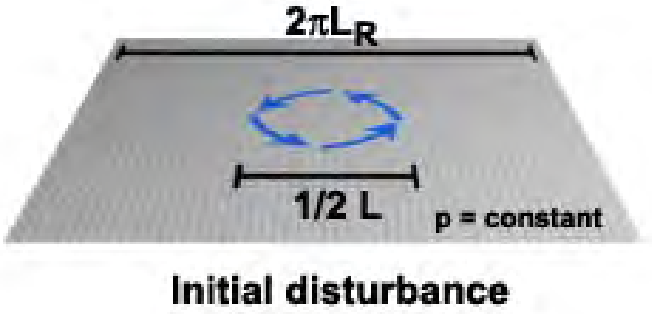

Initial disturbance

Final adjusted state

Parameter study of the atmospheric circulation of Earth-like planets with general circulation models (GCMs)

Williams (1988)

Zonal velocity

white : eastward

shade : westward

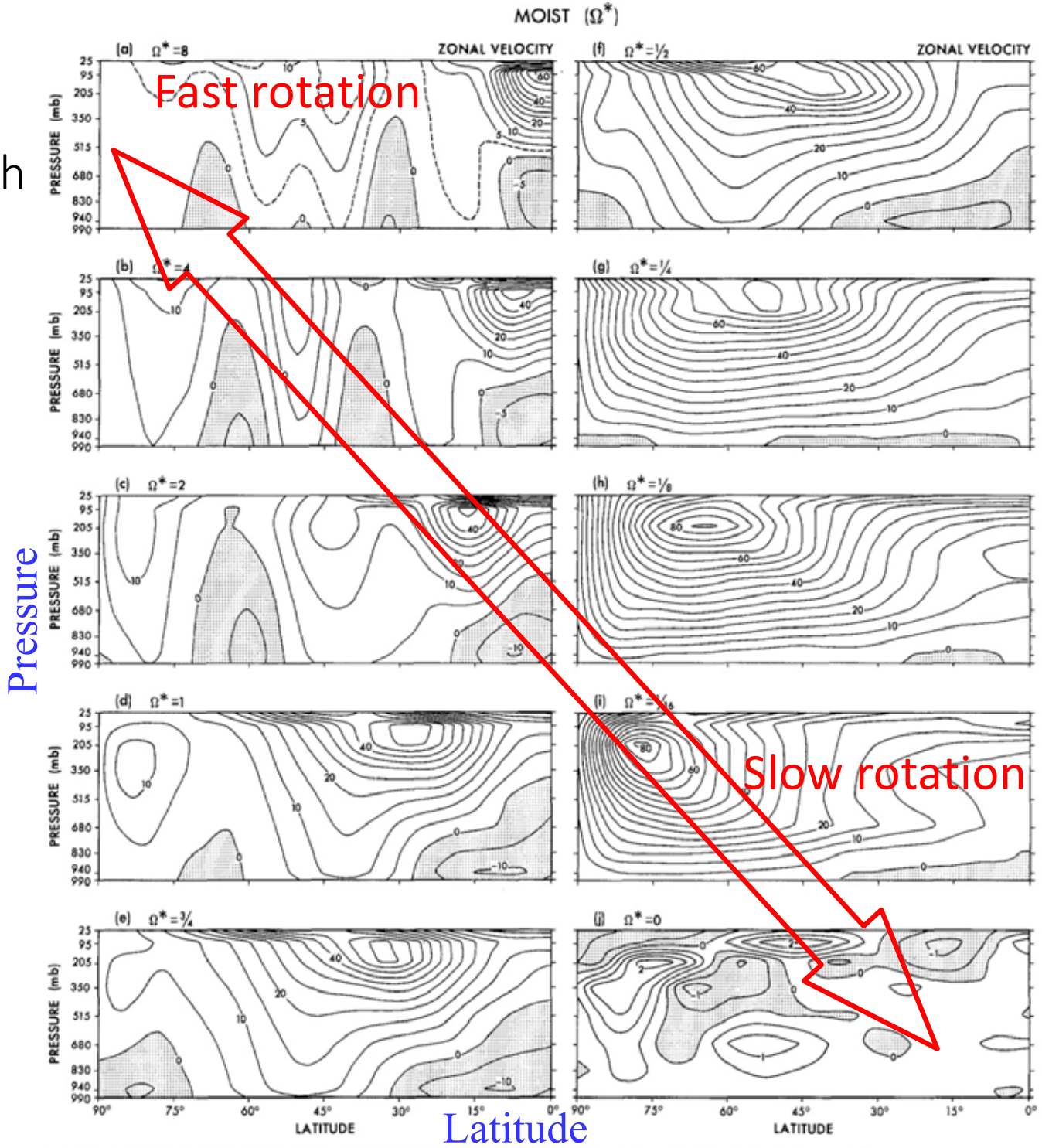

Fig. 2. Meridional distribution of the mean zonal wind for the MOIST model with $\Omega^* = 0$–8. Units: m s^{-1}

Meridional stream function

white : anti-clockwise

shade : clockwise

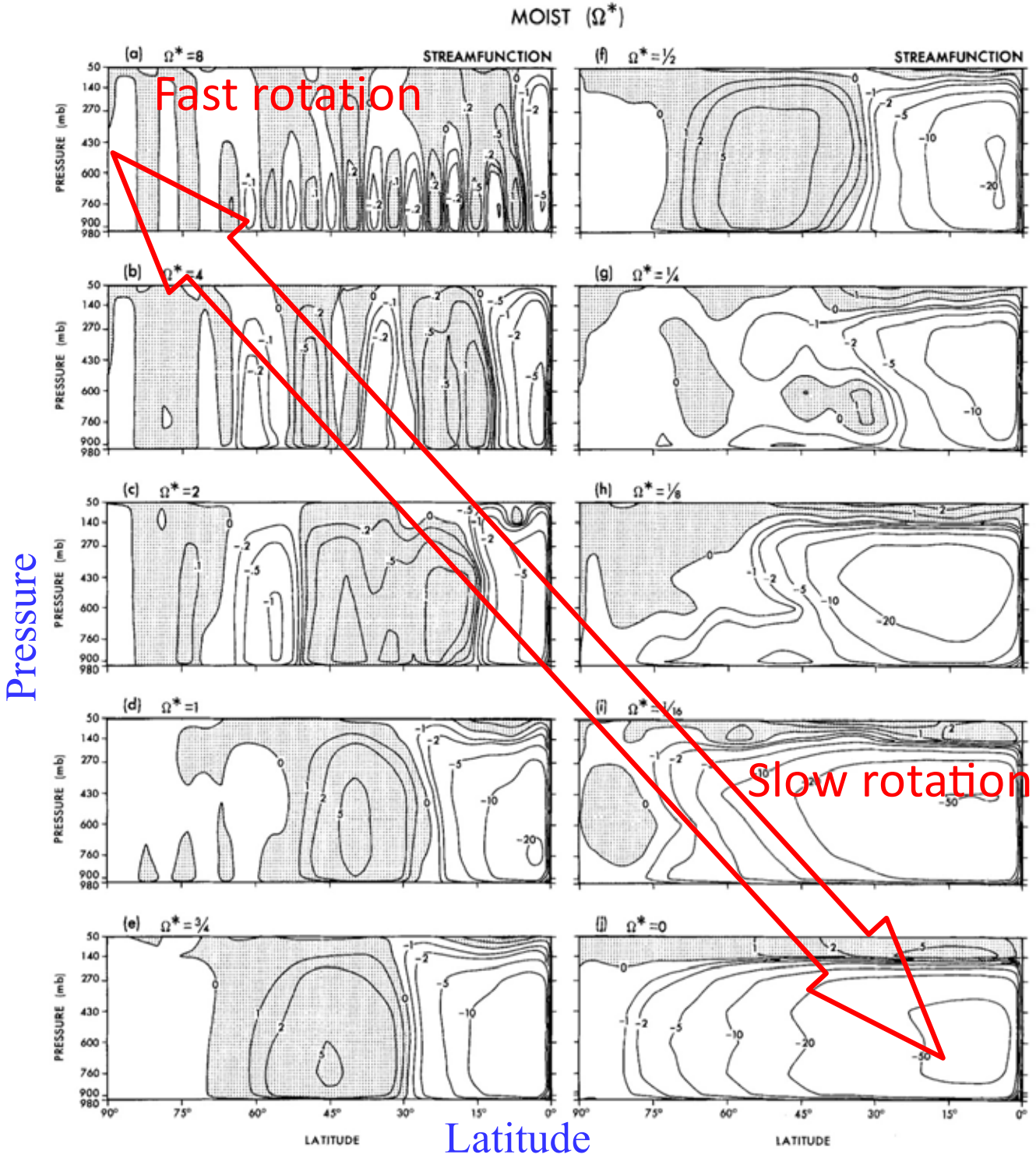

Fig. 3. Meridional distribution of the mean stream function for the MOIST model with $\Omega^* = 0$–8. Units: 10^{13} g s^{-1}

Temperature

white : > 220K

shade : < 220 K

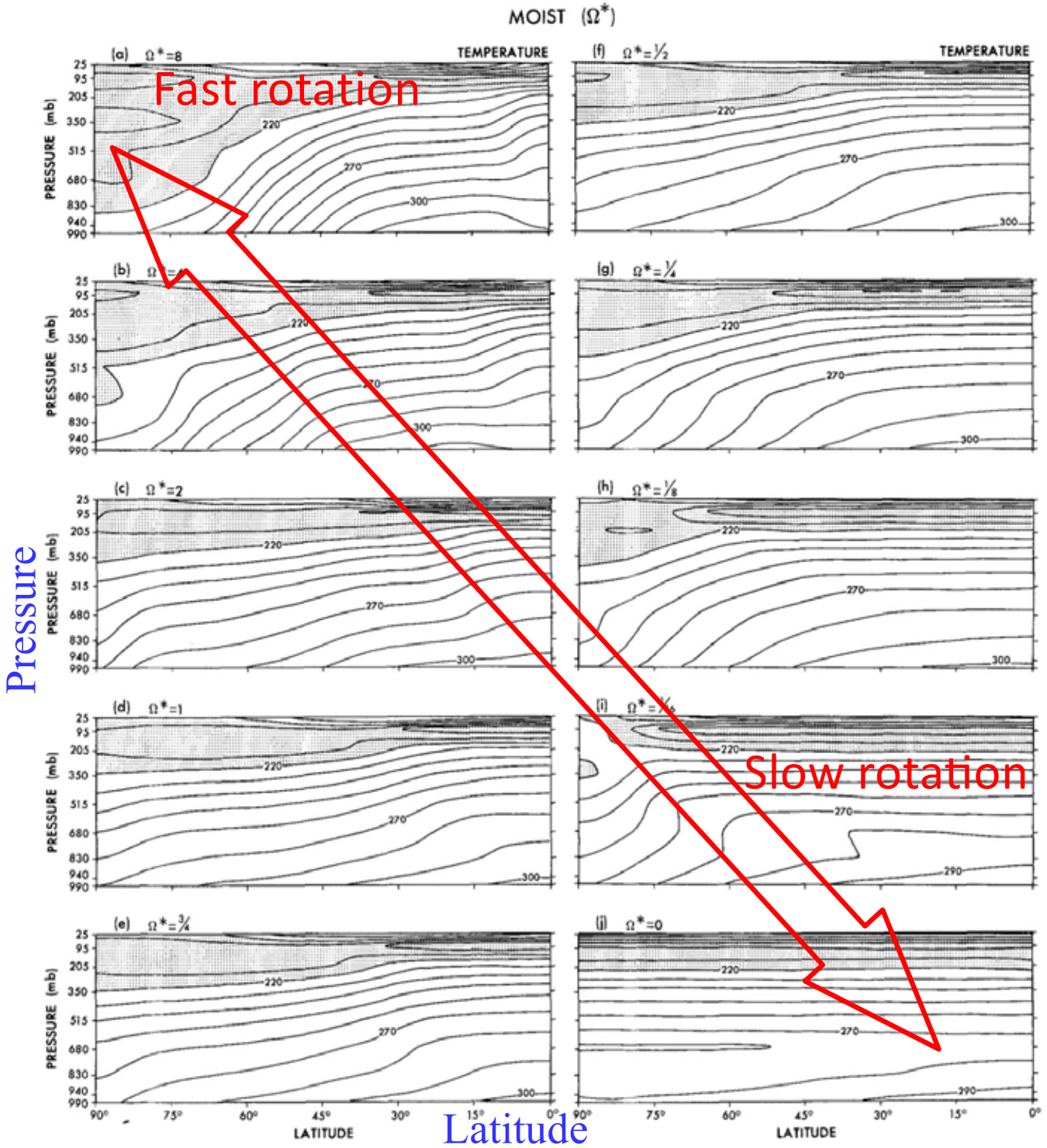

Fig. 4. Meridional distribution of the mean temperature for the MOIST model with Ω* = 0–8. Units: K

Superrotation

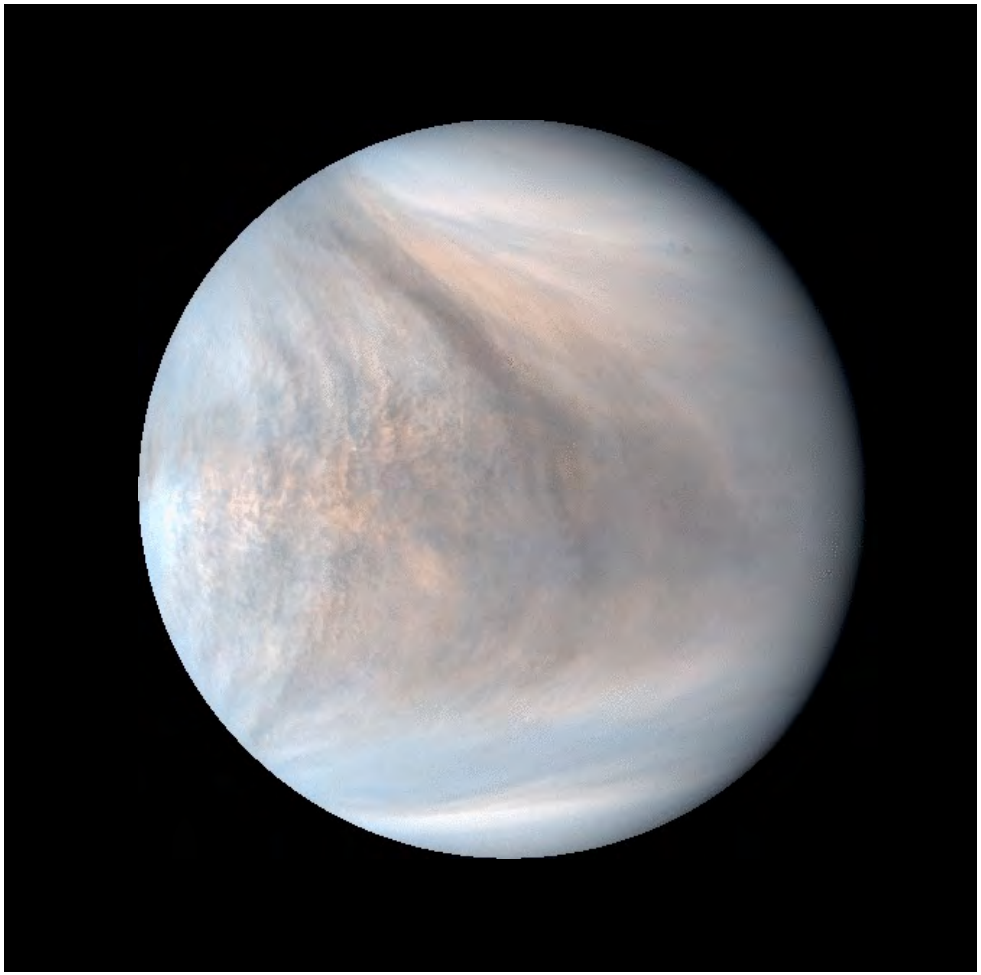

taken by Akatsuki UV Imager

Observed superrotating atmospheres

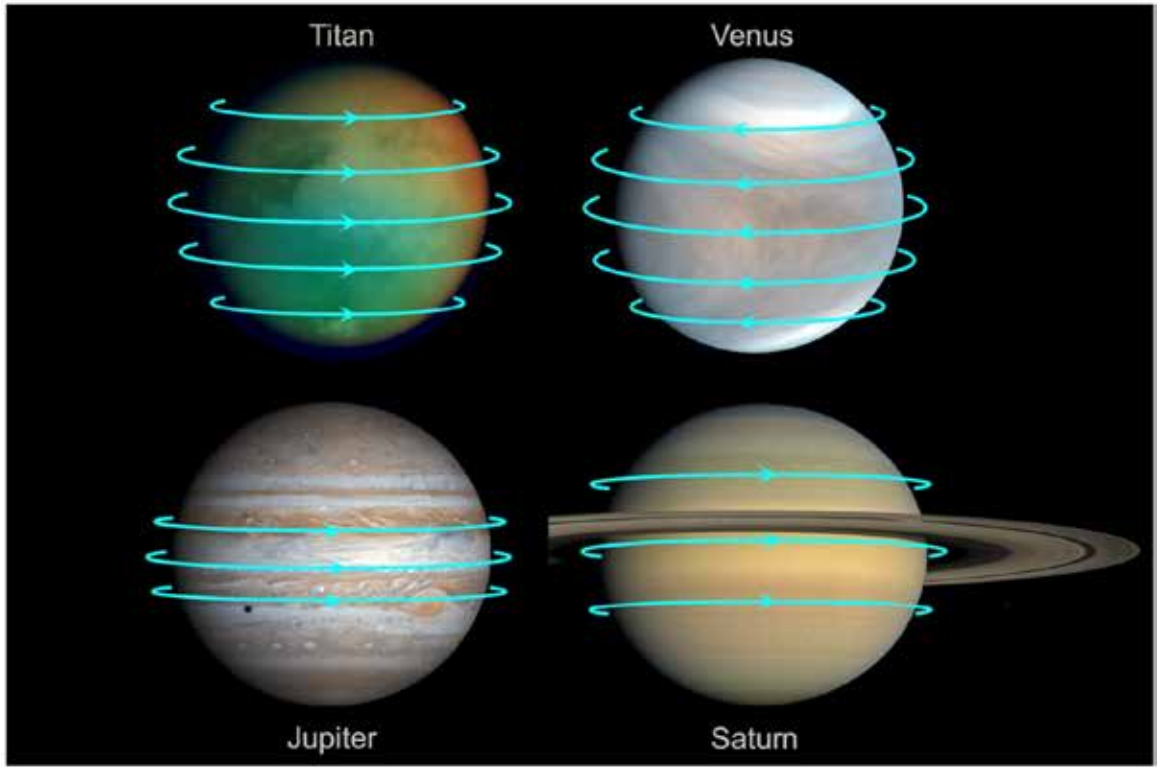

Planet	Radius (km)	Rotation period (days)	Equatorial rotation speed (m/s)	Equatorial wind speed (m/s)	Superrotation index, s, on the equator
Venus	6,052	243	1.81	100–120	55–66
Titan	2,576	16.0	11.7	100–180	8.5–15
Jupiter	69,911	0.41	12,300	60–140	0.005–0.011
Saturn	58,232	0.44	9,540	350–430	0.037–0.045
HD 189733b	79,500	2.2	2600	2400	0.92

Imamura et al. (2020, *Space Sci. Rev.*)

Superrotation of Venus' atmosphere

Zonal winds measured by entry probes

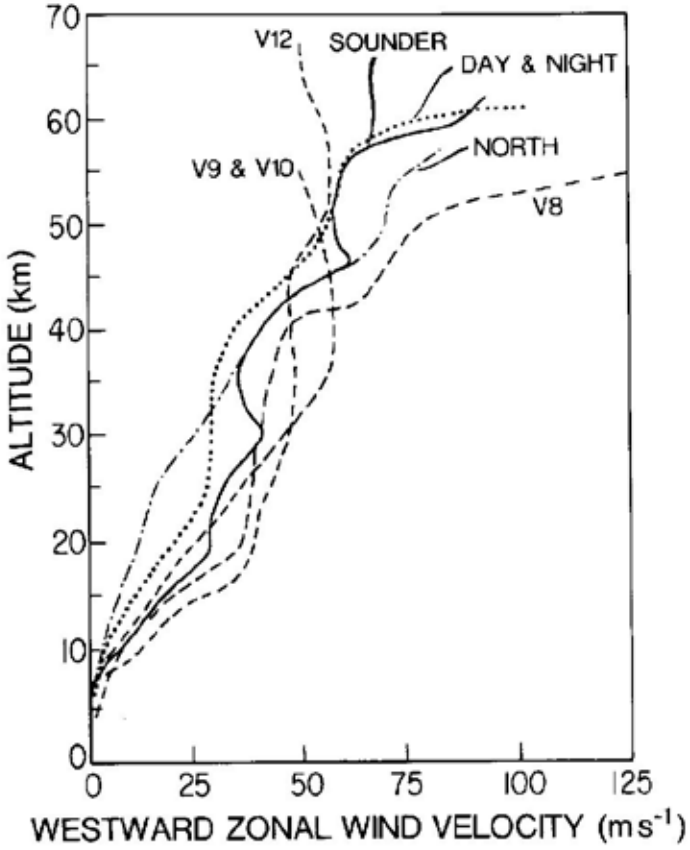

60 times faster rotation of the atmosphere (period=4 Earth days) than the solid planet (period=243 Earth days)

Superrotation of Venus' atmosphere

Latitudinal profiles of the zonal wind speed at different levels (20–60 km) measured by entry probes

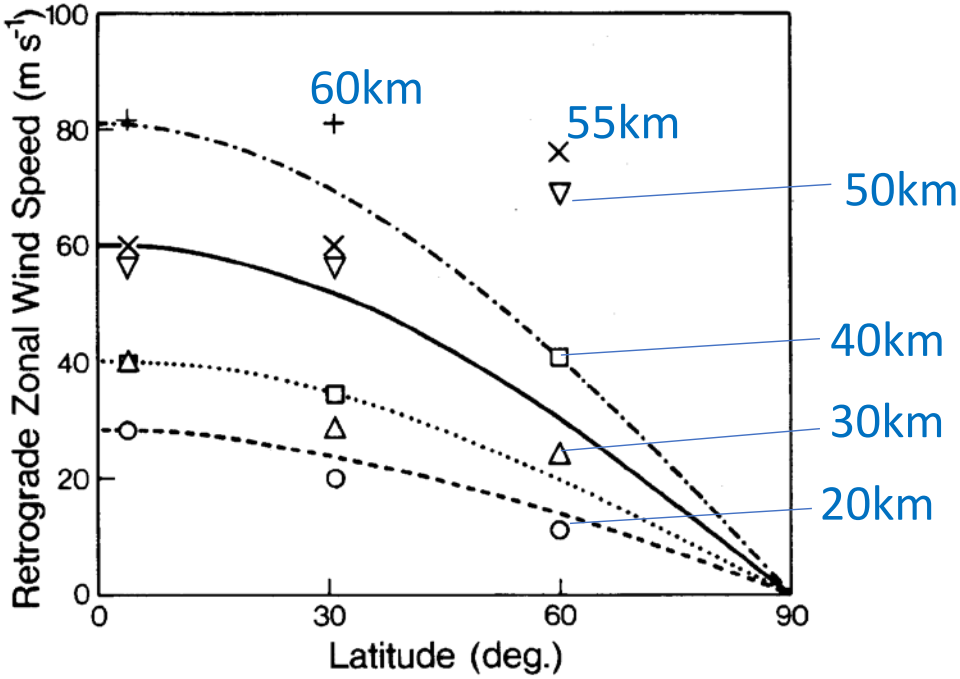

Fig. 10. Latitudinal variation of retrograde zonal wind speeds measured by interferometric tracking of Pioneer Venus probes. The symbols refer to different altitudes: 20 km, (0); 30 km, (Δ); 40 km, (□); 50 km, (▽); 55 km, (×); and 60 km, (+). The curves represent solid body rotation at different rates. It is assumed that the zonal circulation is approximately symmetric about the equator, so the wind speeds for the Day and Night probes can be plotted at 31°N.

Cloud-tracked winds from various missions

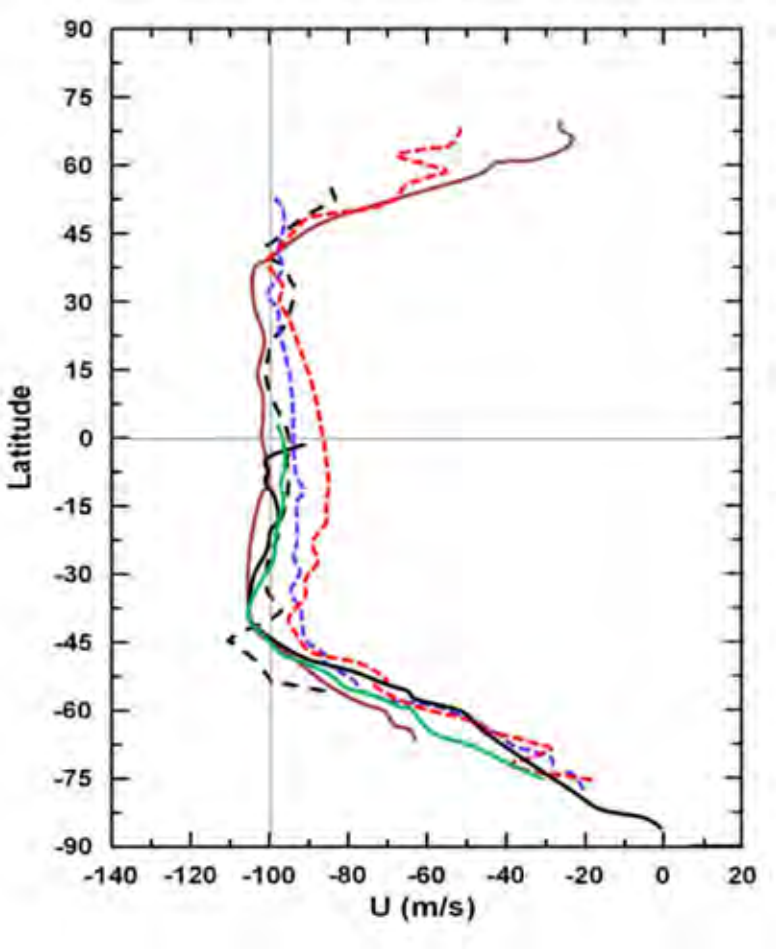

Sánchez-Lavega et al. (2017)

Superrotation of Titan' atmosphere

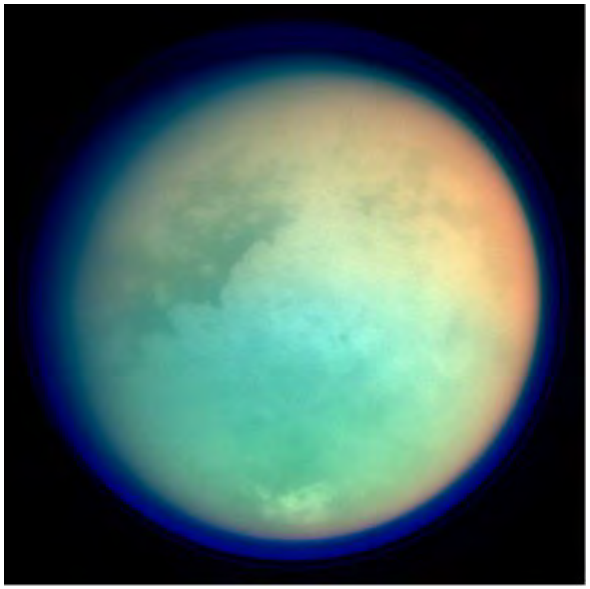

Hörst et al. 2017

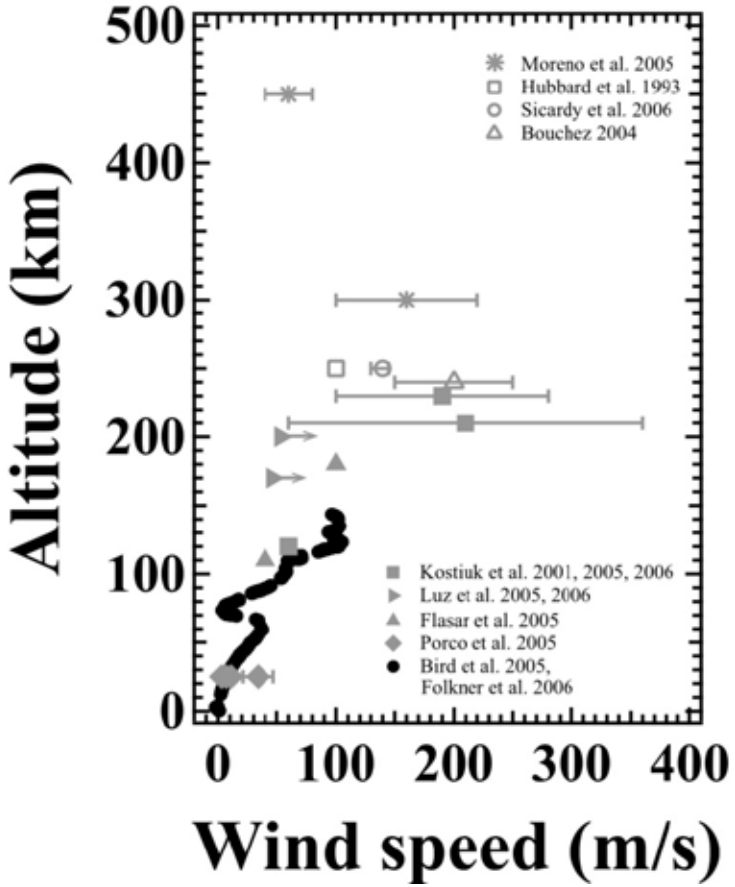

The atmosphere circulates 10 times faster than the rotation of the solid planet.

Infrared observation by CIRS on NASA Cassini

(northern winter)

Achterberg et al. 2008

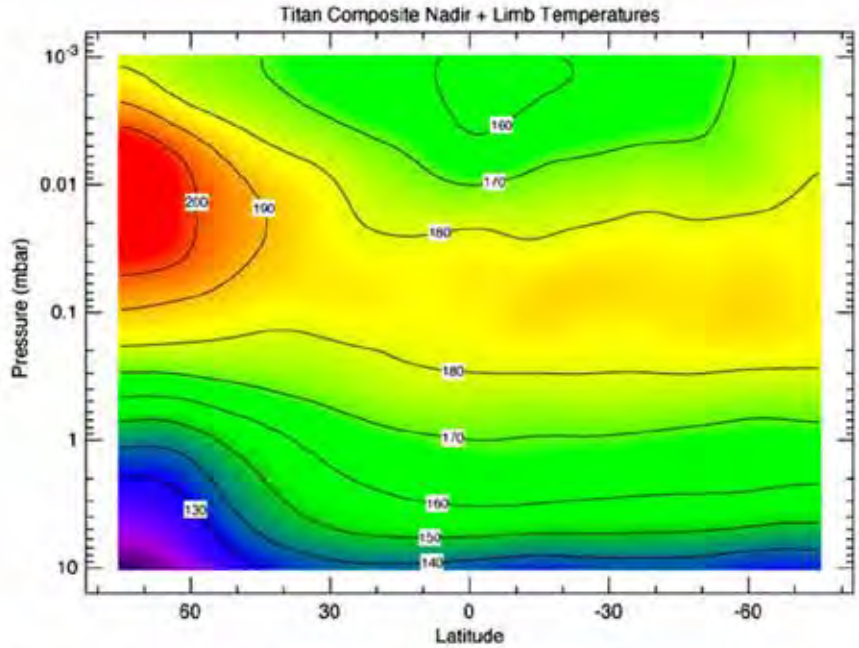

Zonal-mean temperature

Fig. 9. Zonal mean temperatures from all limb and nadir maps. Retrieved temperatures were averaged in 5° latitude bins, then smoothed with a 10° boxcar function applied three times. Contours are labeled in K.

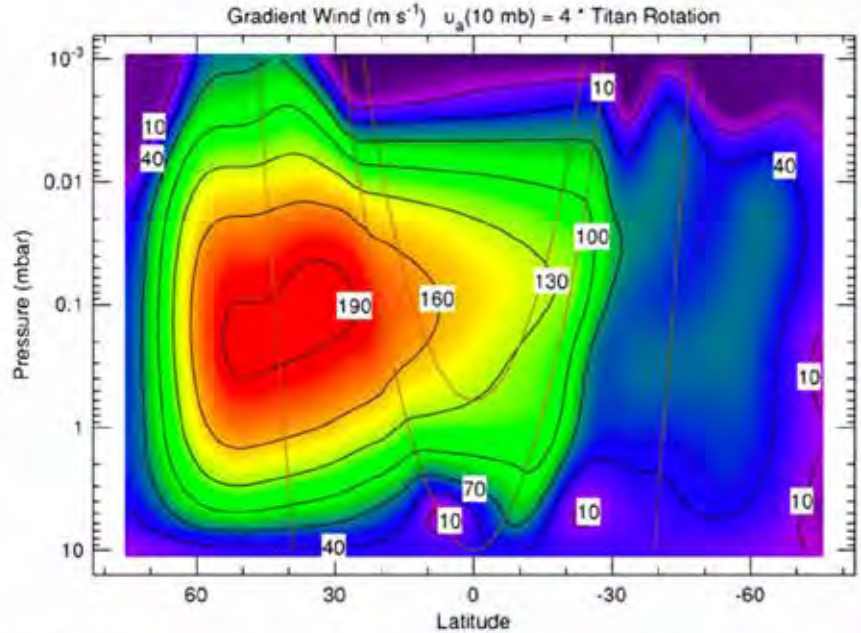

Zonal winds calculated from the temperature using thermal wind relation

Fig. 10. Zonal winds calculated from the temperatures in Fig. 9 from the gradient wind equation, assuming solid-body rotation at the 10 mbar level at four times Titan's rotation rate. Wind speed contours (black lines) are labeled in m s^{-1}. The gray lines indicate cylindrical surfaces parallel to the rotation axis along which the gradient wind equation is integrated. Equatorward and above the gray line tangent to the equator at 10 mbar, the winds are unconstrained by the gradient wind equation, and have been linearly interpolated on constant pressure surfaces.

$$R_o \equiv \frac{U}{fL}$$

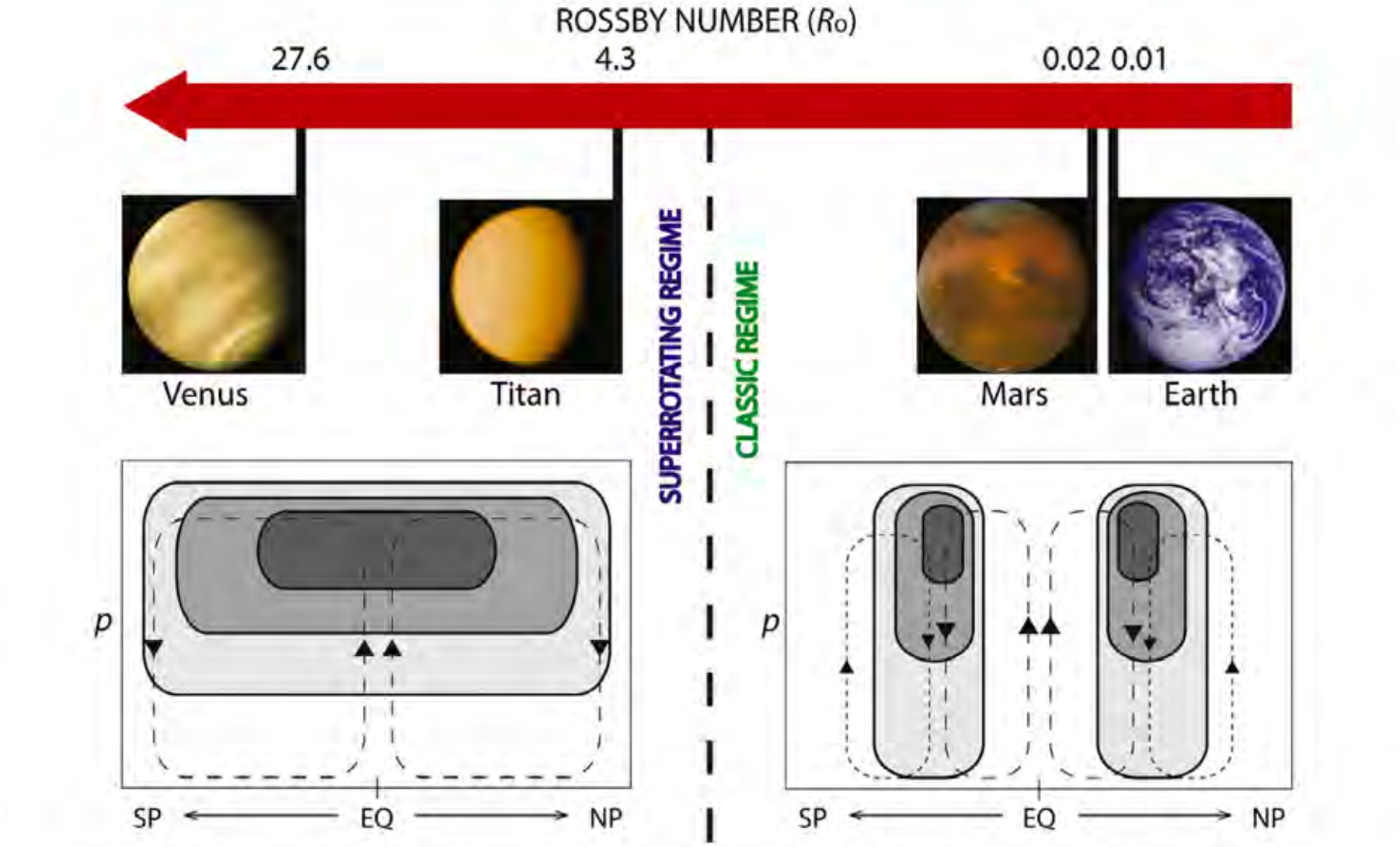

Fig. 1. Schematic view of the different Rossby numbers (R_O) and circulation regimes found on the terrestrial bodies of the Solar System with substantial atmospheres. R_O was computed based on typical scales of zonal winds (around 100 m s^{-1} for Venus and Titan and 10 m s^{-1} for Earth and Mars), rotation rate, and planetary radius. The lower panels depicts a hypothetical vertical cross section of zonal mean zonal wind (shaded, arbitrary scale) and mean overturning circulation (dashed lines, arbitrary scales) characteristic of each body's atmospheres. See text for more details (photo credits: NASA/JPL).

Dias Pinto & Mitchell (2014)

Hide's theorem

Hide (1969) showed that non-axisymmetric eddies (waves) are needed to maintain the jets aloft the surface and that the required momentum convergence should be provided by upgradient angular momentum transport.

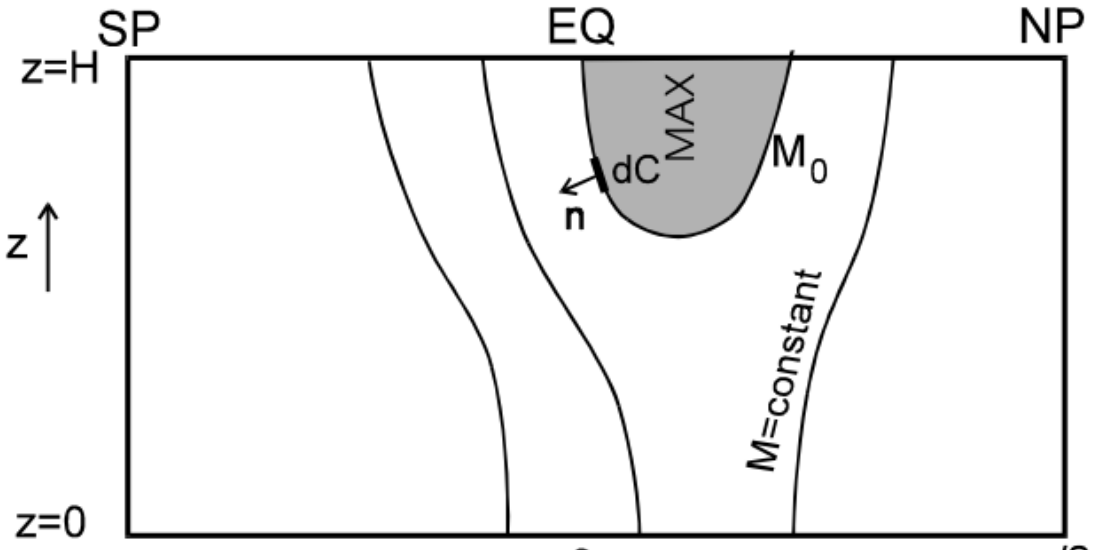

(Vallis, 2005)

Hypothesis: Acceleration by meridional circulation and horizontal eddies (Gierasch, 1974; Rossow & Williams, 1979)

Hadley circulation

transports angular momentum poleward, thereby creating high-latitude jets.

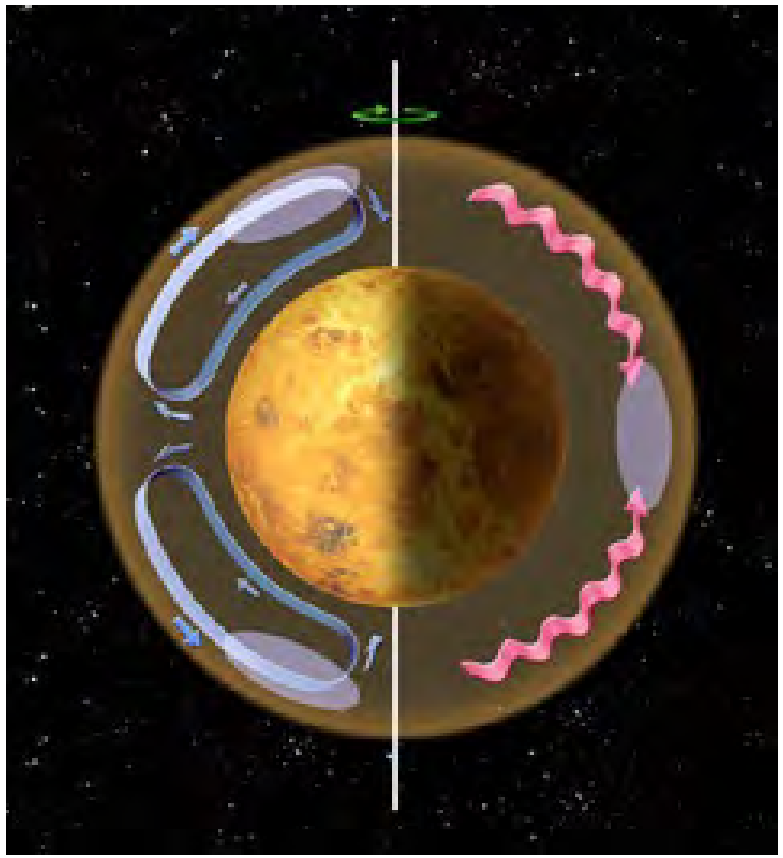

Horizontal eddies

transport angular momentum equatorward to smooth out the differential rotation of the atmosphere.

The combination of the two processes leads to an accumulation of angular momentum in the equatorial upper atmosphere.

2D simulation in a slowly-rotating system

（Williams and Rossow　1979)

- planetary rotation same as Venus
- momentum forcing at high latitudes

→ baroclinic instability, followed by generation of large-scale waves and equatorward momentum transport

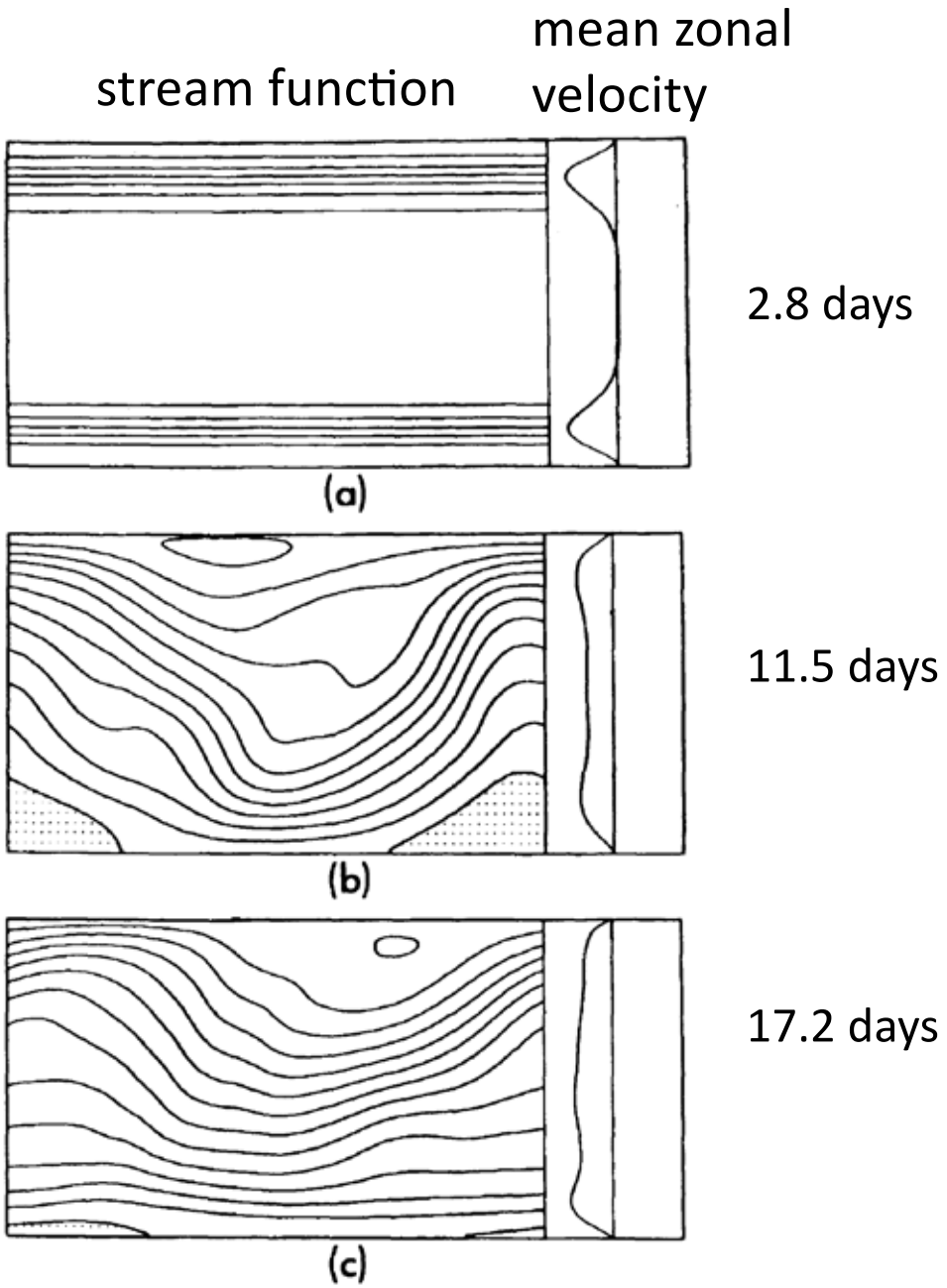

Difference in wave characteristics between Earth and Venus

	Earth	Venus
		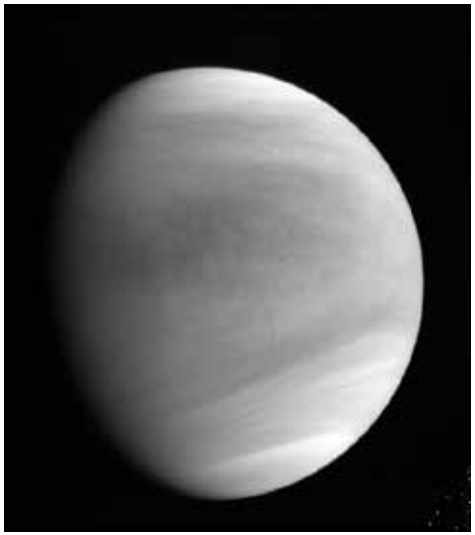
Rotation period	1 day	243 days
	↓	↓
	Small waves	Large waves
	↓	↓
	Poleward AM transport	?

Rossby radius of deformation

$$L_R = \frac{\sqrt{gH}}{f}$$

g : gravitational acceleration
H : depth of the system
$f = 2\Omega \cos\theta$: Coriolis parameter

The characteristic scale at which the velocity field and the pressure field adjust with each other to maintain geostrophic flow

Faster planetary rotation leads to large f, and then shorter L_R

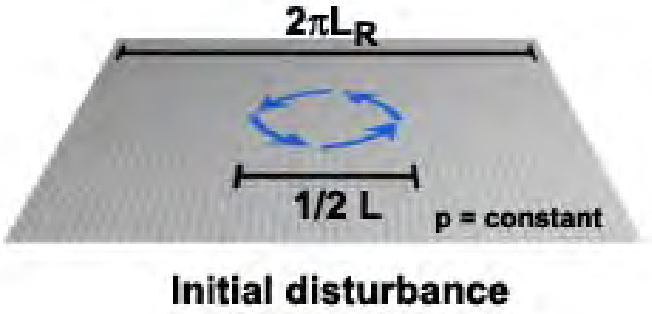

Initial disturbance

Final adjusted state

Rossby-Kelvin instability

(Sakai 1989; Iga and Matsuda 2005; Wang & Mitchell 2014)

Coupled mode seen in a Titan-like GCM (Wang & Mitchell 2014)

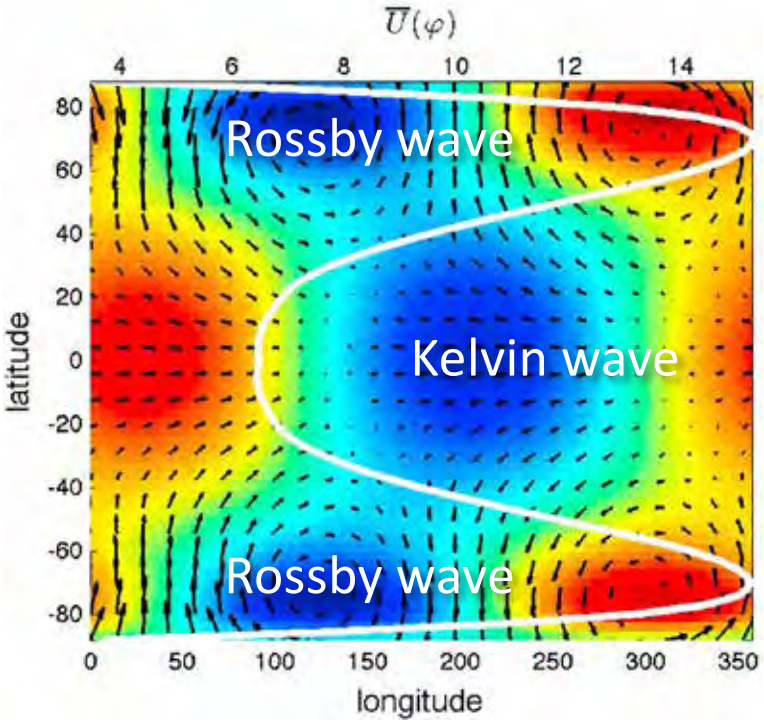

Coupled mode seen in a Venus GCM (Takagi et al. 2022)

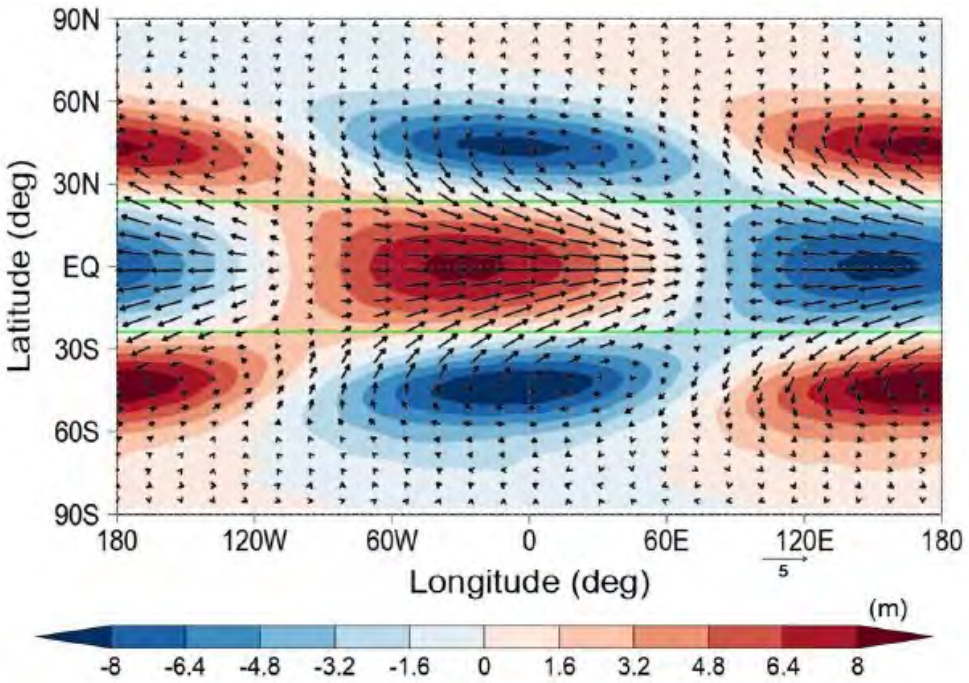

Planetary-scale shear instability can transport angular momentum equatorward

Parameter dependence in Earth-like GCM (Dias Pinto & Mitchell 2014)

Zonal velocity

Meridional circulation
Temperature

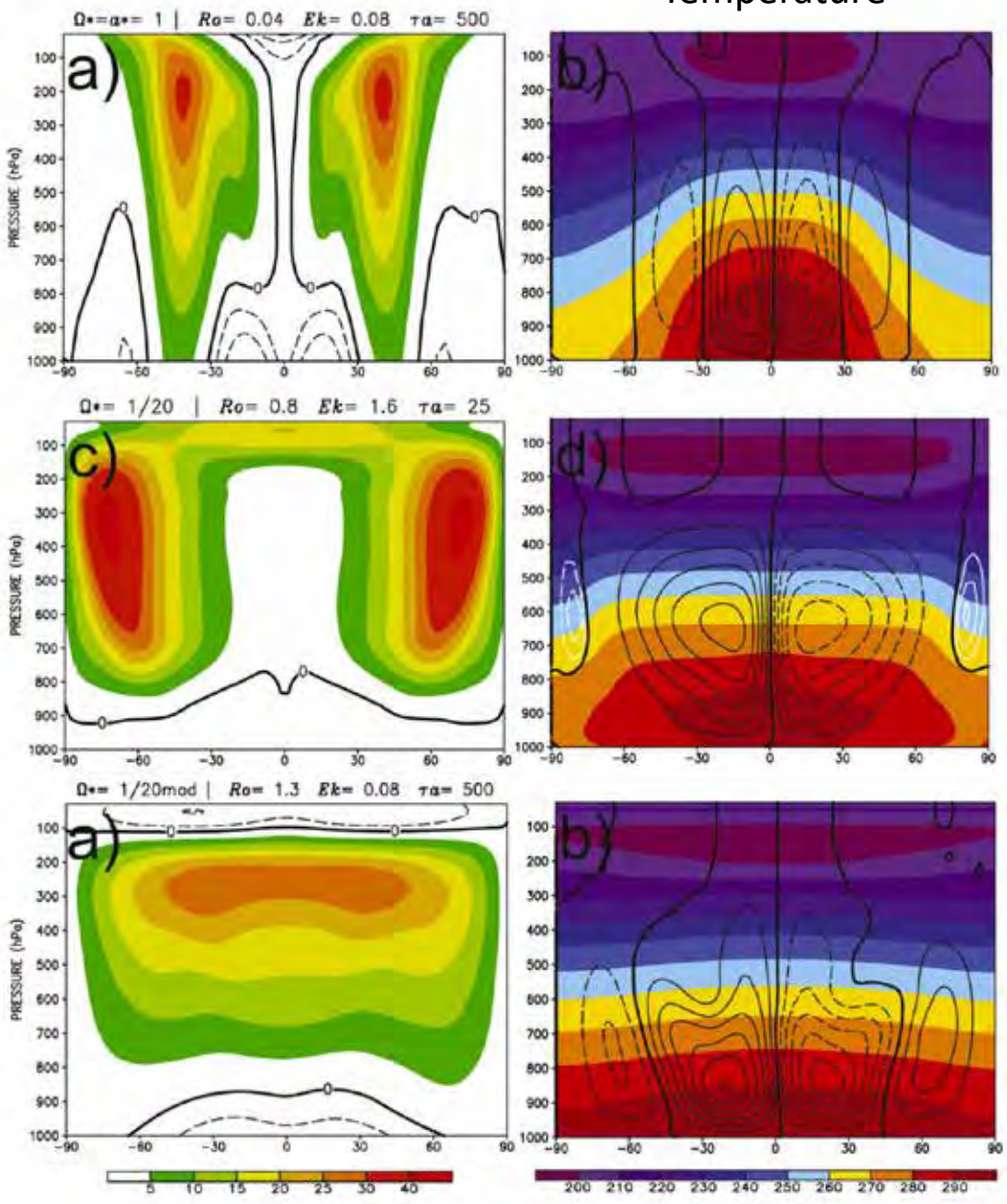

Earth' condition $R_o = 0.04$

Rot. rate x 1/20 $R_o = 0.8$

Hadley cell spreads, but superrotation does not develop because of the relatively short radiative/viscos time scale.

Rot. rate x 1/20 $R_o = 1.2$
Relaxation time x 20

Superrotation develops when the radiative/viscos time scales are made longer.

Radiative relaxation time

- The time scale over which the atmosphere is warmed by solar radiation or cooled by emitting infrared radiation.
- It is considered that the meridional circulation is determined by this time scale.

- The larger the heat capacity of the atmosphere, the longer the radiative relaxation time.
  - Mars

    Surface pressure = 0.006 bar → Relaxation time ~ 3 Earth days
  - Earth

    Surface pressure = 1 bar → Relaxation time ~ 100 Earth days
  - Venus

    Surface pressure = 92 bar → Relaxation time ~ 50 Earth years

Conditions for superrotation

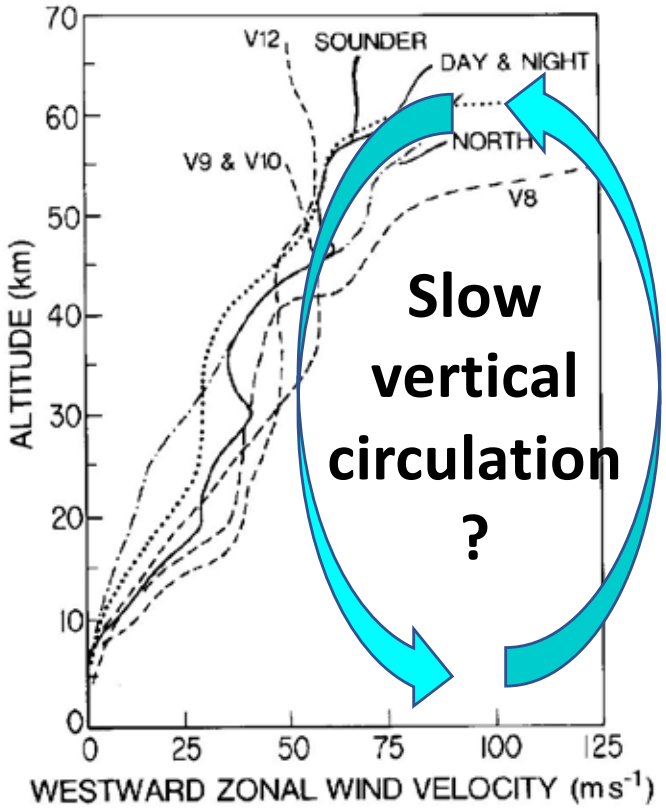

- ✓ Slow planetary rotation
  - On slow-rotating planets, atmospheric waves caused by planetary-scale dynamical instabilities unknown in Earth's meteorology lead to an acceleration of the atmosphere.
    (When the planet rotates rapidly, atmospheric waves accelerate the atmosphere at high latitudes like the Earth)
- ✓ Long radiative relaxation time
  - A dense atmosphere has a large heat capacity and a longer relaxation time. The vertical circulation slows down, making it difficult to smooth out the velocity change with altitude and making it easier to maintain the superrotation.

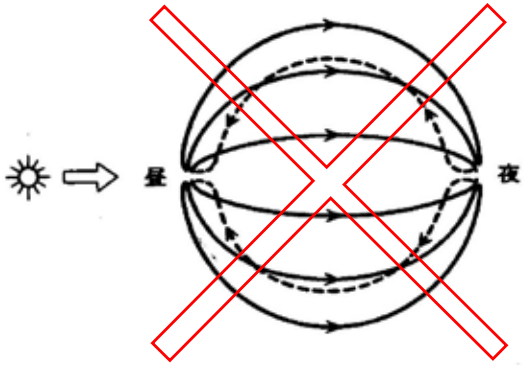

Opposite extreme = Mars

Short-timescale effect of the lower atmosphere to the upper atmosphere

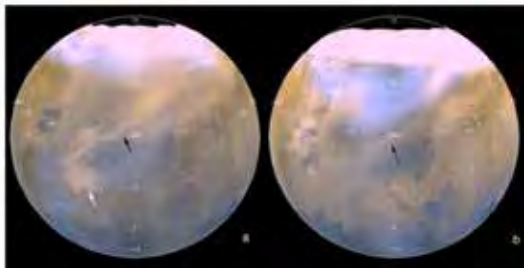

Frontal dust storms (Wang et al. 2005)

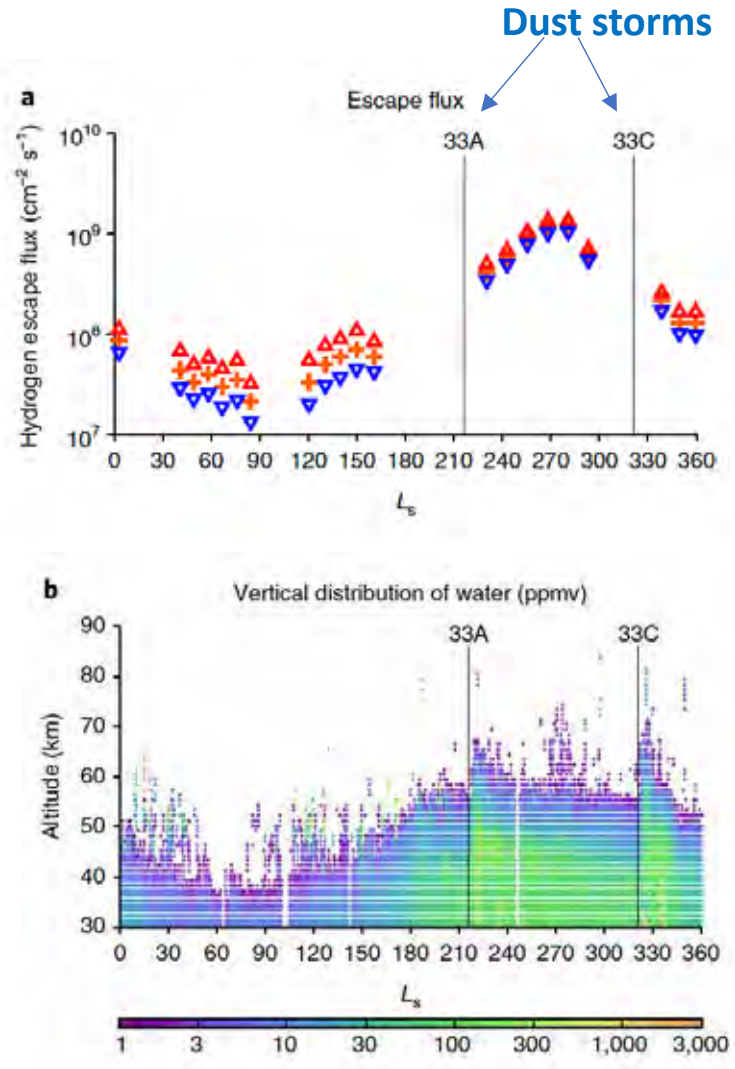

Hydrogen escape observed by MAVEN Solar Wind Ion Analyzer

Vertical distribution of water vapor observed by Mars Reconnaissance Orbiter MCS

Heavens et al. (2018)

Venus

Mars

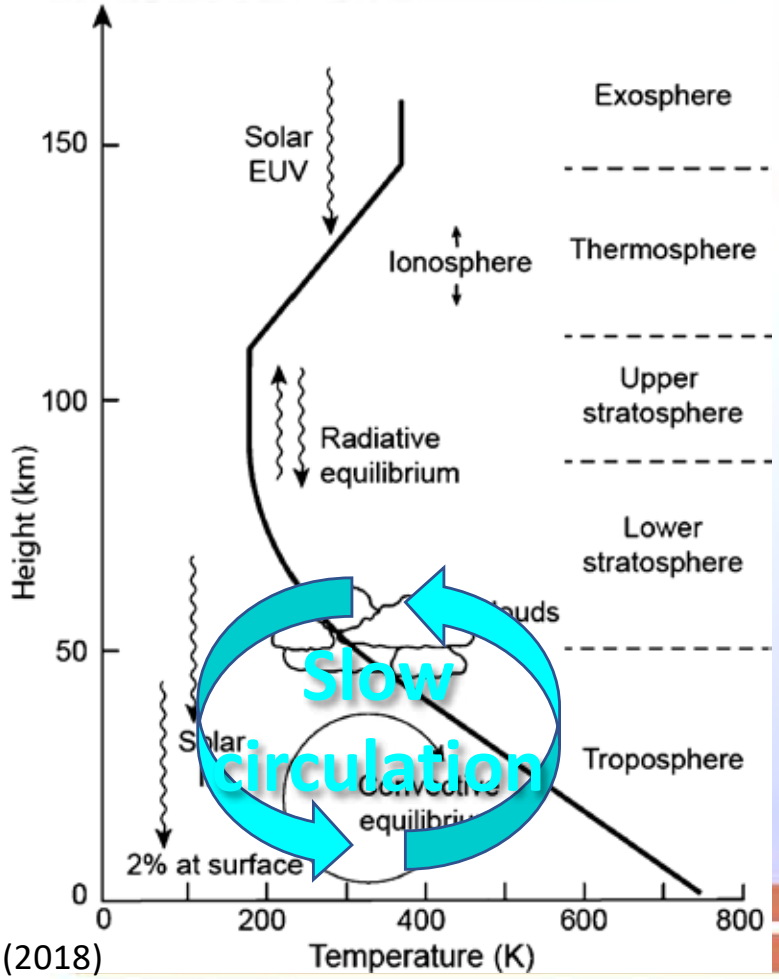

Taylor (2018)

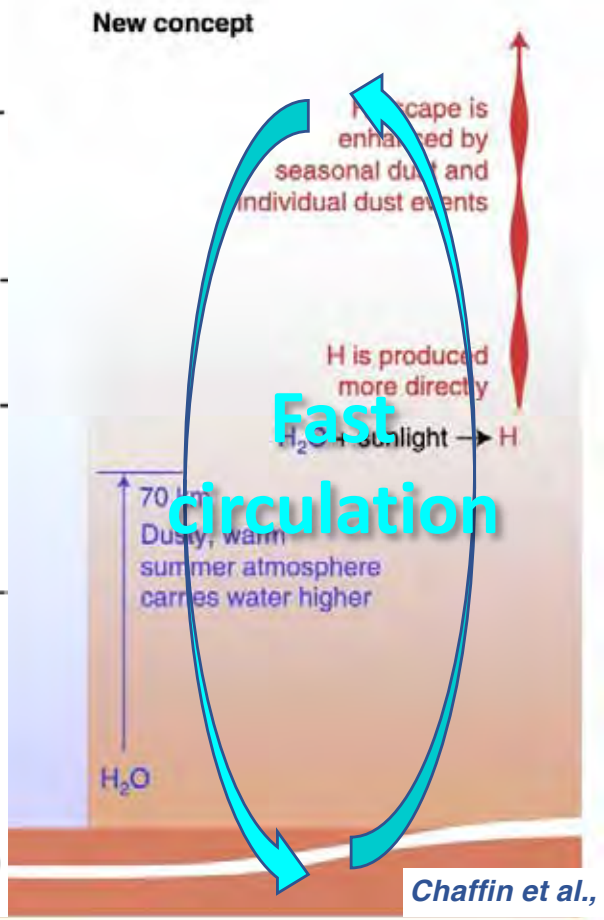

Chaffin et al., 2021

Another mechanism: Acceleration by thermal tides

(Fels & Lindzen 1974)

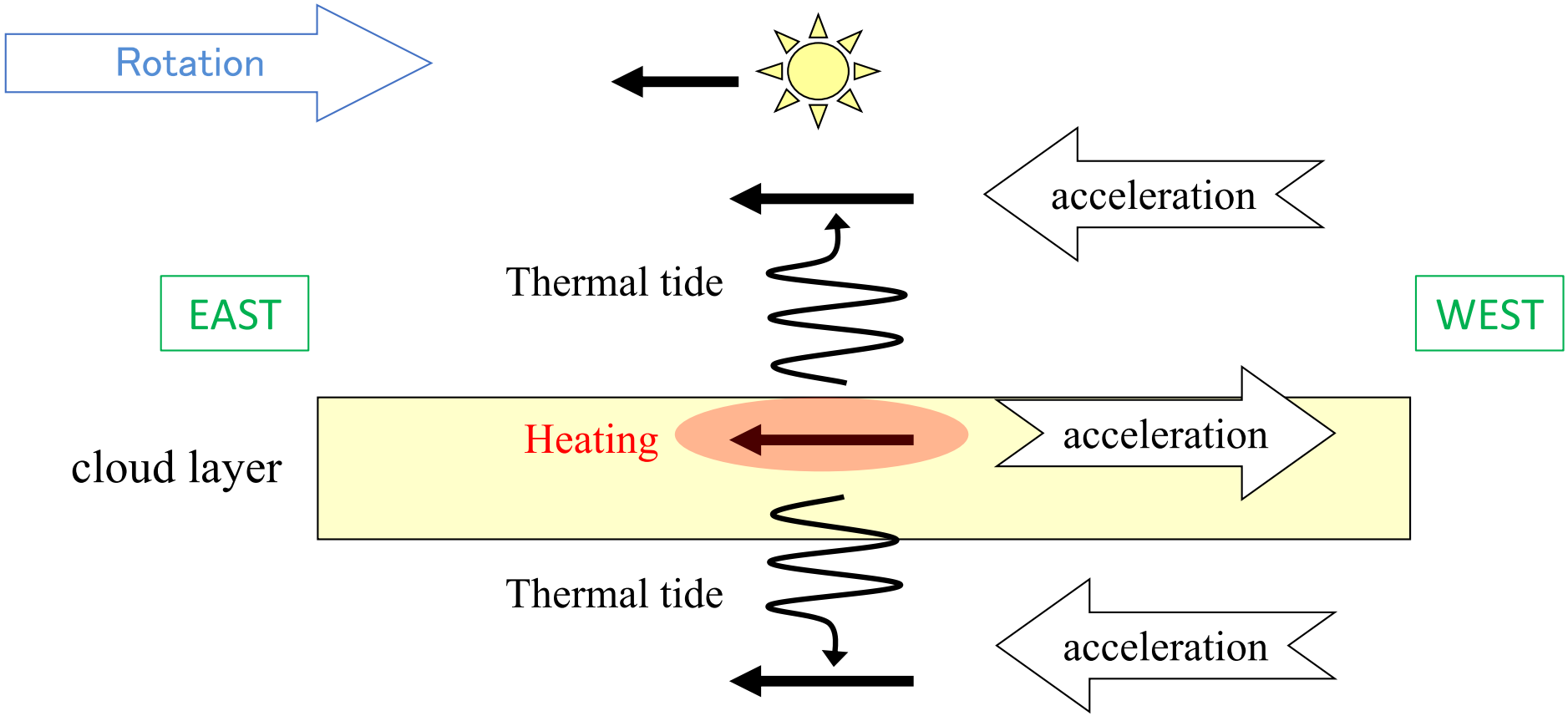

Eastward movement of the solar heating region in the cloud generates thermal tides (planetary-scale gravity wave) → The tides having eastward momentum propagate upward and downward → Vertical redistribution of momentum leads to a westward acceleration of the cloud-level atmosphere

Vertical structure of thermal tides in Venus's atmosphere

Linear solution (Takagi & Matsuda, 2006)

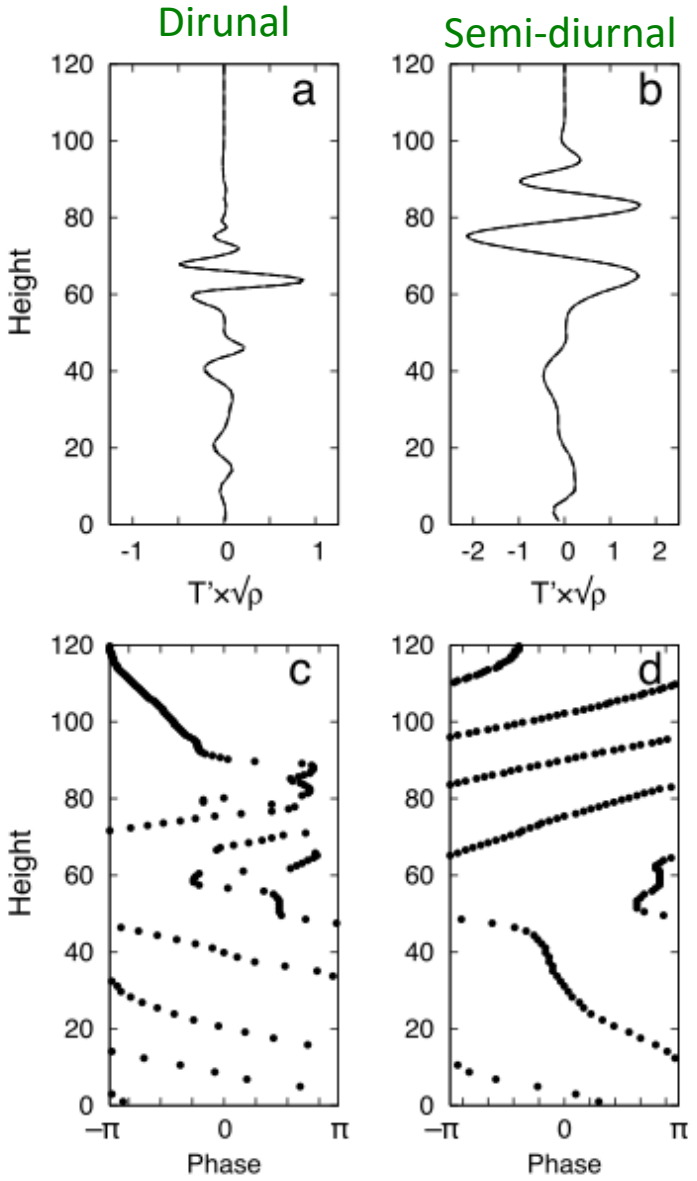

Temperature perturbation
(Schofield & Taylor 1983)

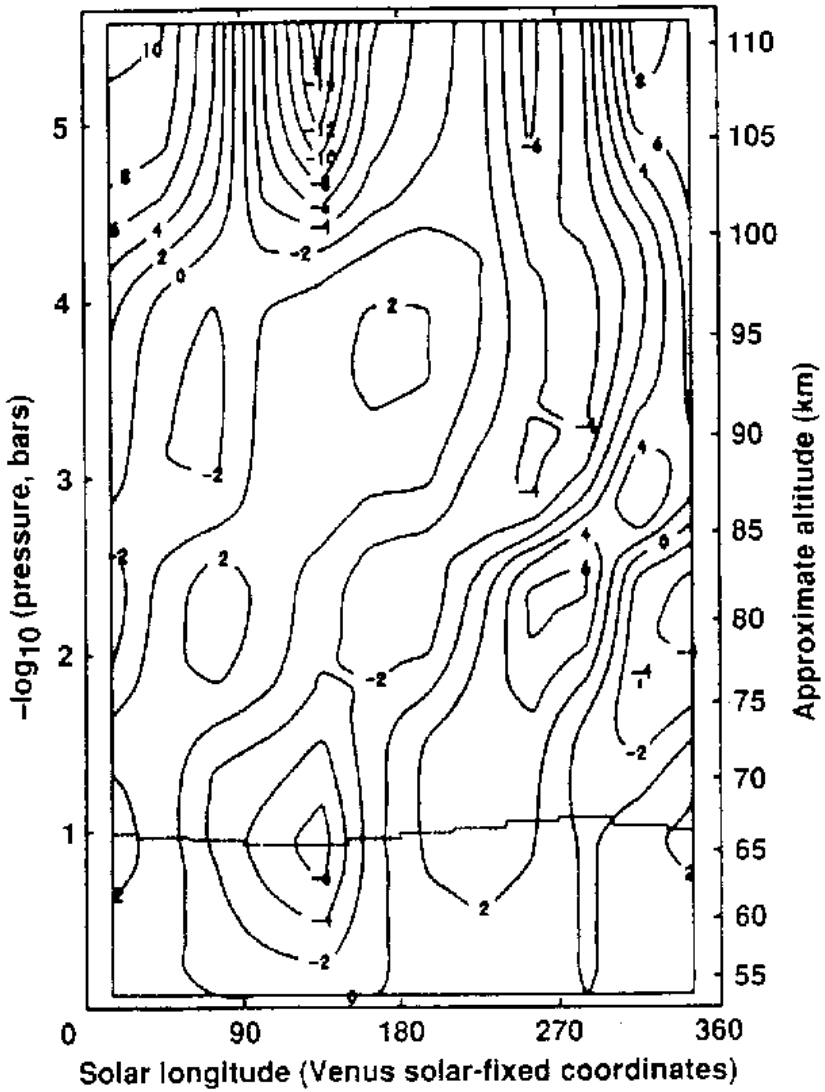

Wind field of thermal tides on Venus (Fukuya et al. 2021)

Clouds seen in thermal IR

Dayside

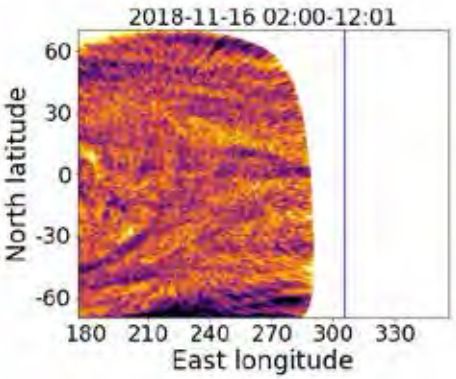

Nightside

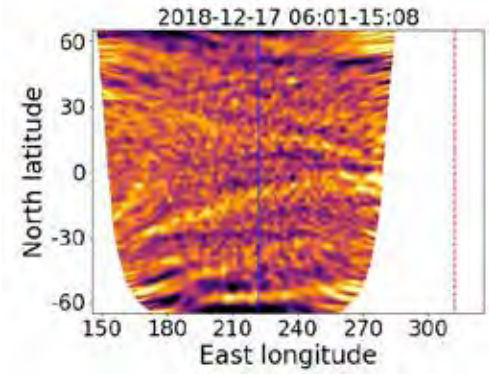

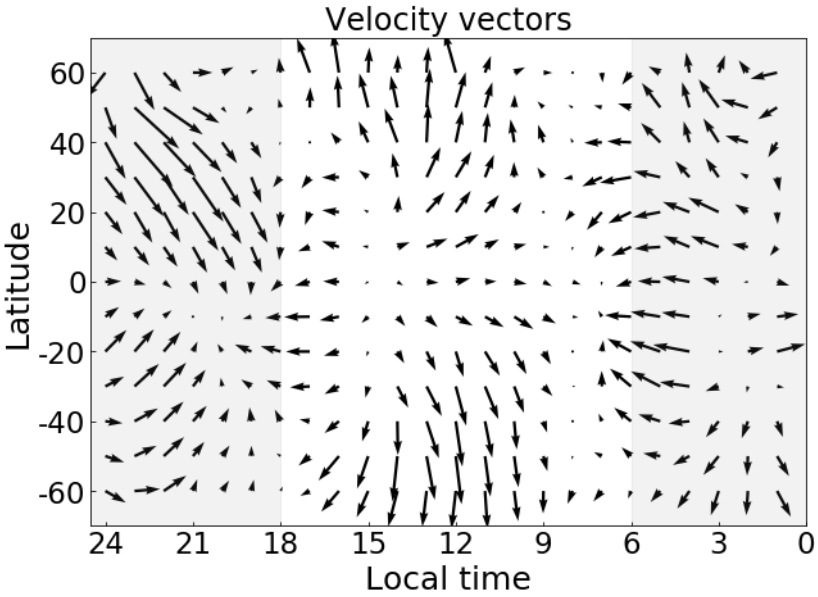

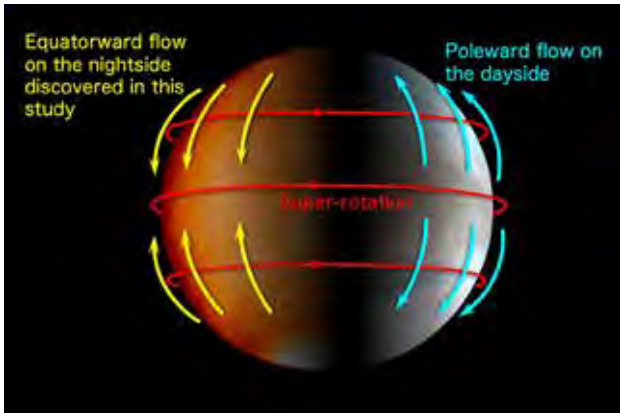

- Equatorward circulation was discovered on the nightside
- Dayside poleward flow and the nightside equatorward flow cancel each other

Numerical models

Zonal winds

Garate-Lopez and Lebonnois (2018)

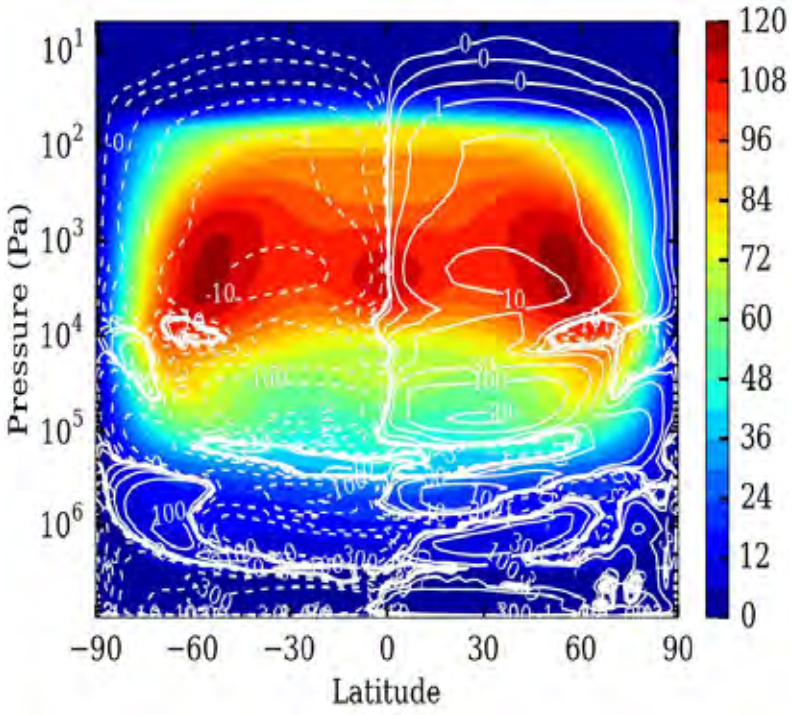

Sugimoto et al. (2014)

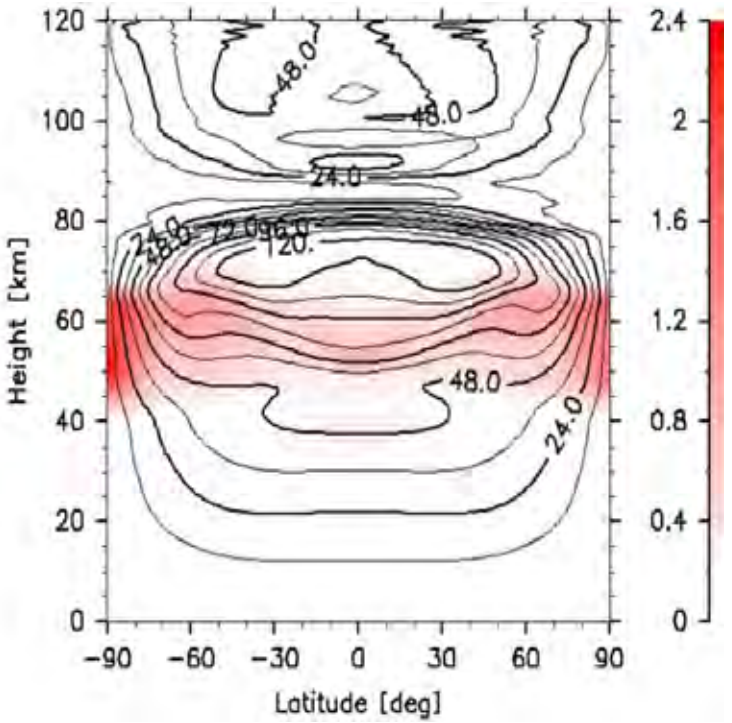

Numerical model of Titan

Lebonnois et al. (2012)

Mean zonal wind and meridional stream function

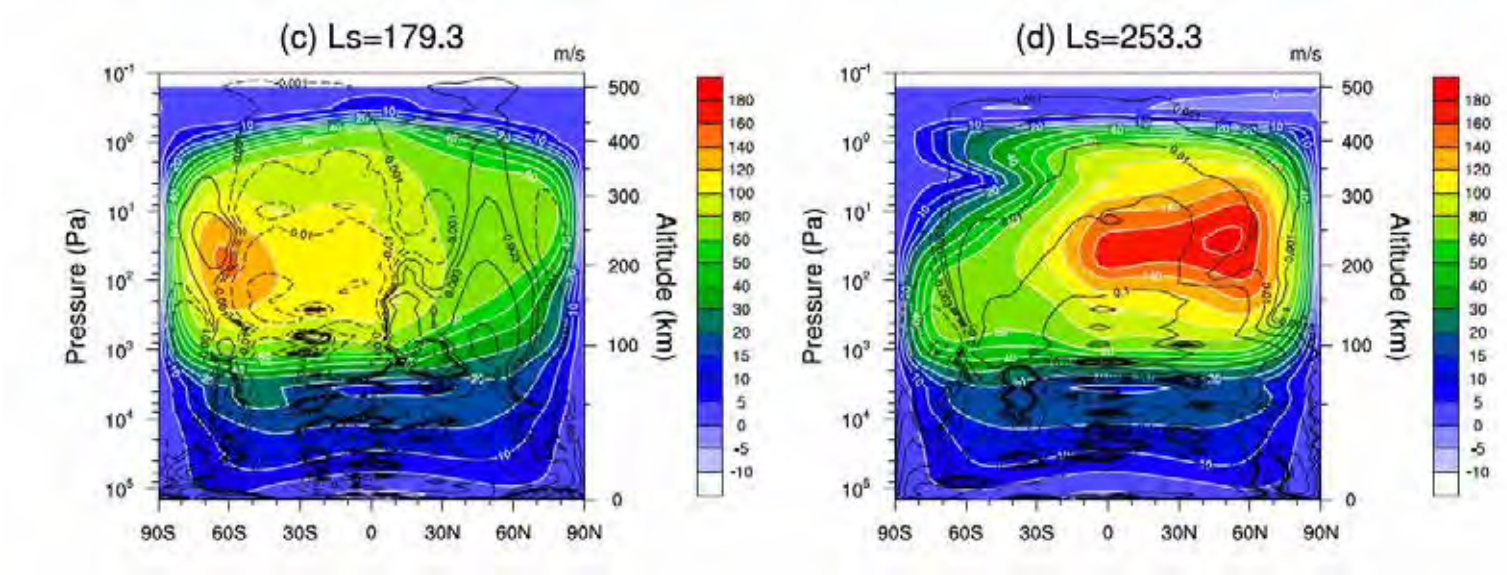

Seasonal variations of the vertically-integrated latitudinal transport of angular momentum

mean meridional circulation

transient waves

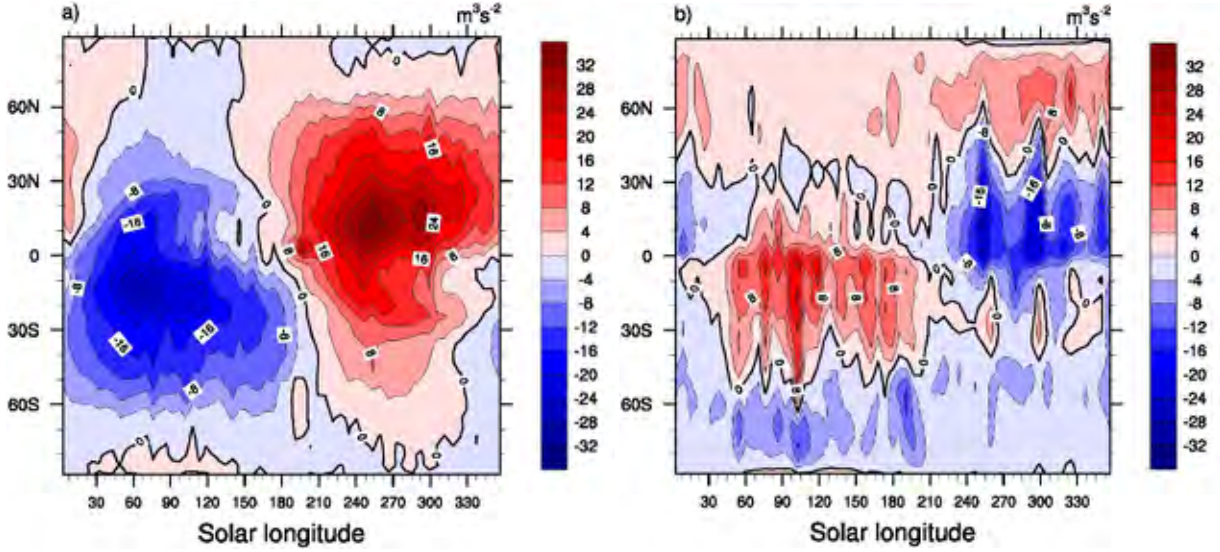

Equatorial superrotation on Mars induced by thermal tides

Wavenumber 1+2 components observed by MCS onboard MRO

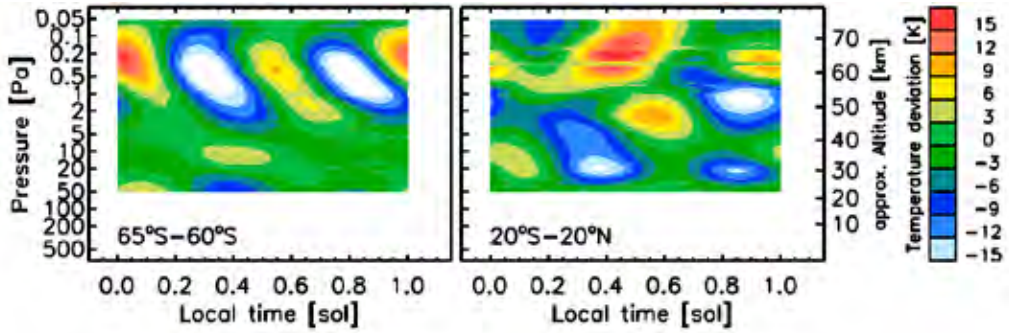

Mars GCM

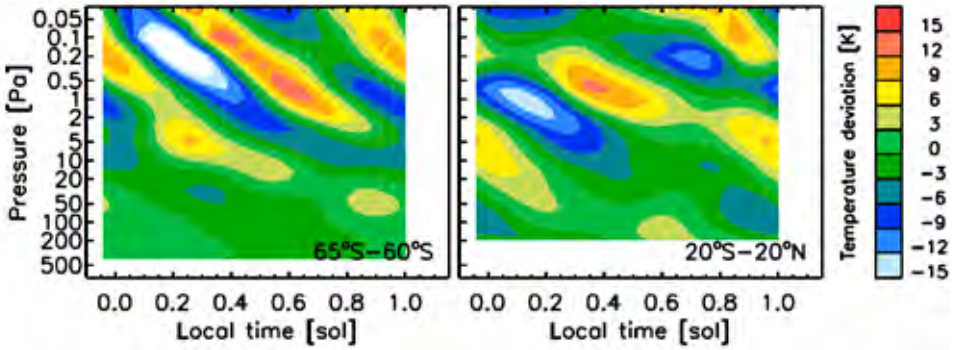

Kleinbohl et al. 2013

Zonal-mean zonal wind in a Mars GCM (dusty period)

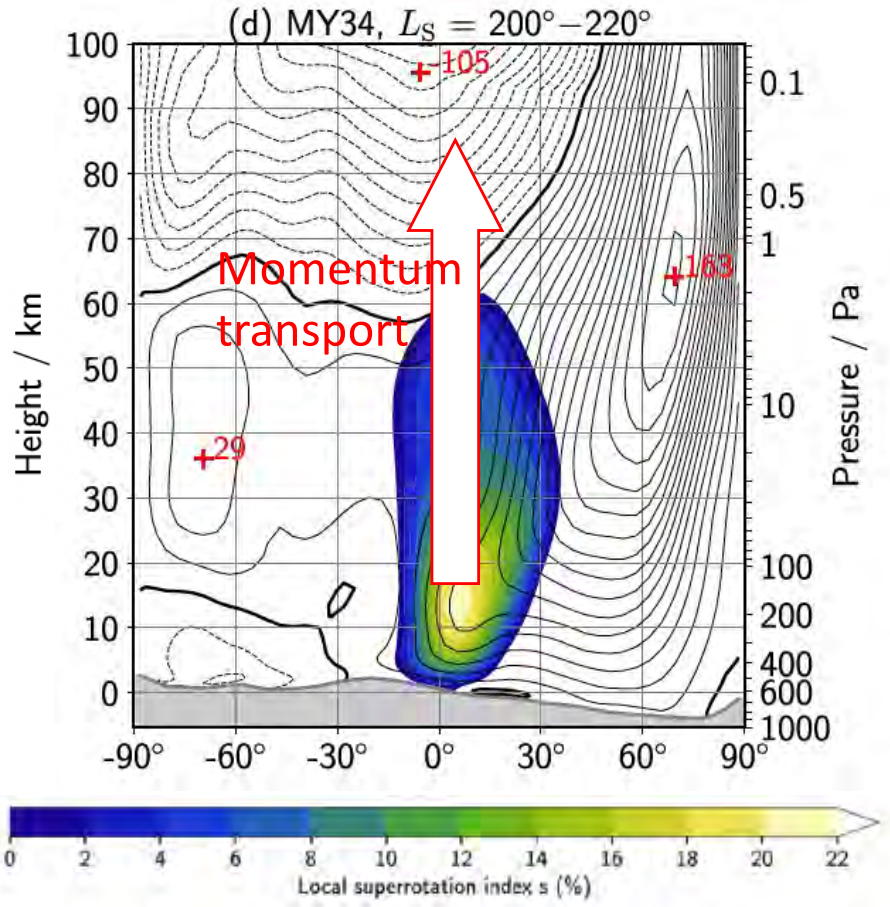

Rajendran et al. 2018

Implications for exoplanets

- Tidally-locked planets are mostly slow rotators like Venus.
- Super-rotation can redistributes thermal energy along the local time on such planets.

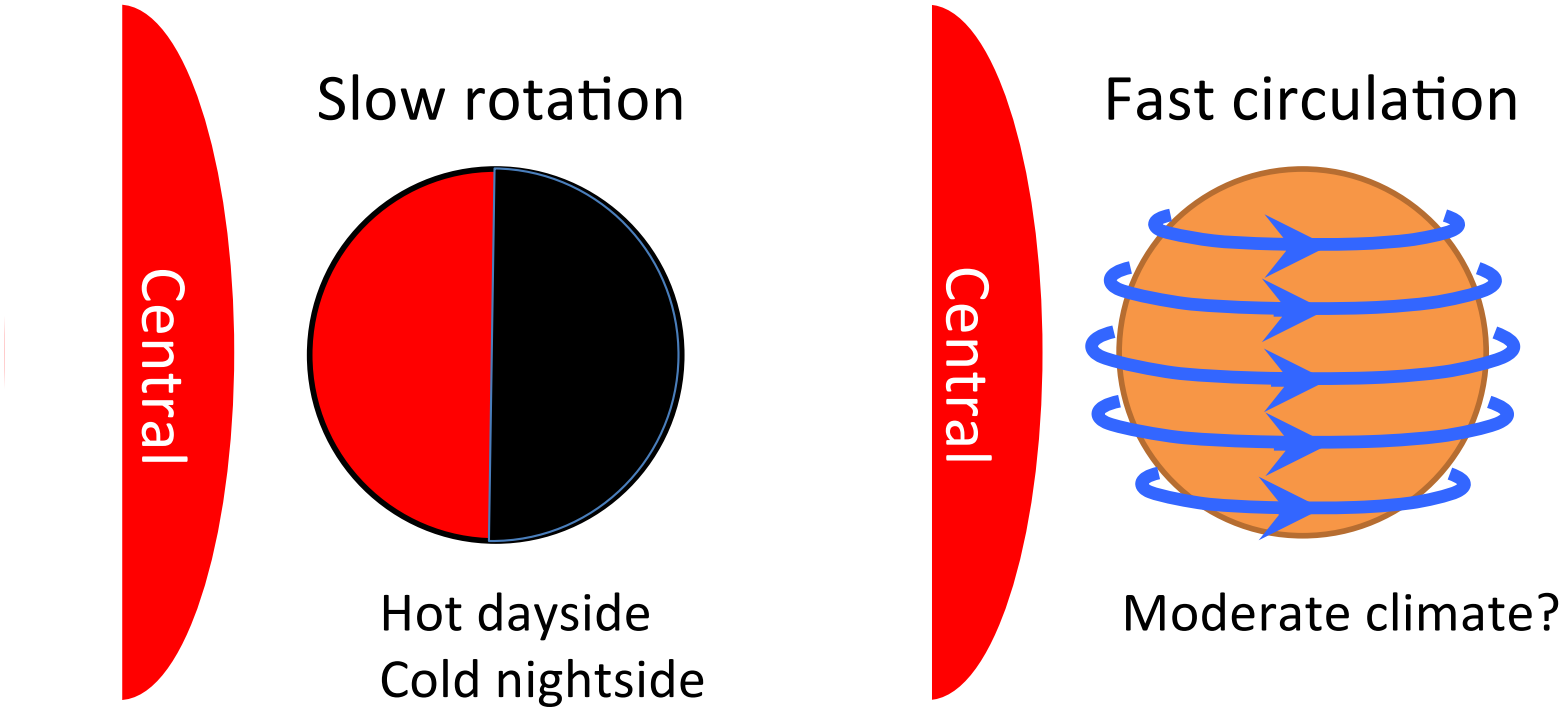

Antisolar

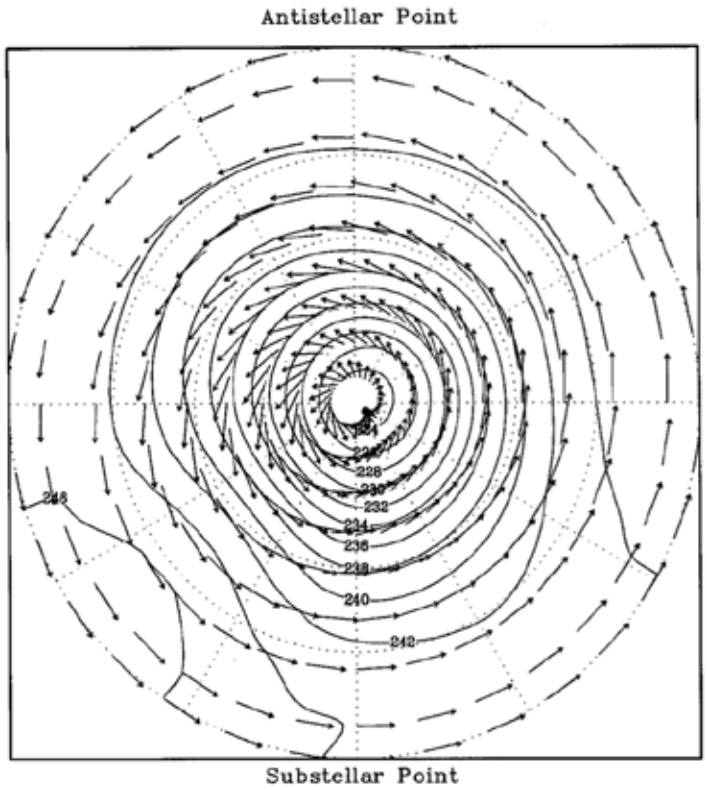

Subsolar

Polar view of the atmospheric circulation and temperature distribution at 20 km altitude on a synchronously rotating terrestrial planet (Joshi et al., 1997)

A map of the day-night contrast of the extrasolar planet HD 189733b (Knutson et al. 2007)

A minimum brightness temperature of 973 +/- 33 K and a maximum brightness temperature of 1212 +/- 11 K at a wavelength of 8 microns, indicating that energy from the irradiated dayside is efficiently redistributed throughout the atmosphere

Observed phase variation for HD 189733b, with transit and secondary eclipse visible.

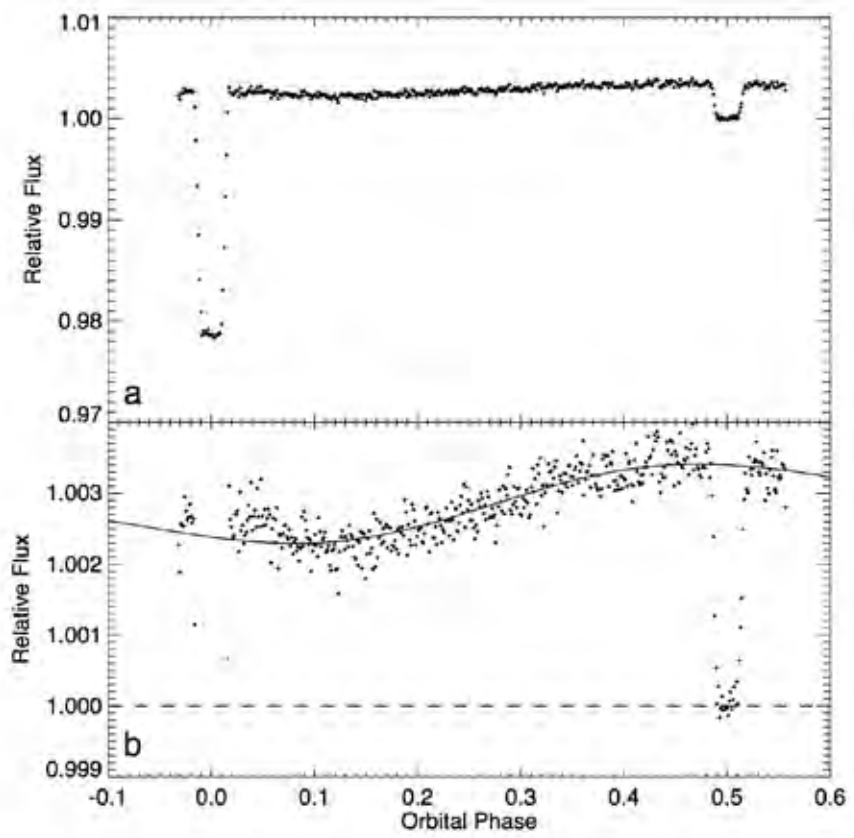

Brightness estimates for 12 longitudinal strips on the surface of the planet

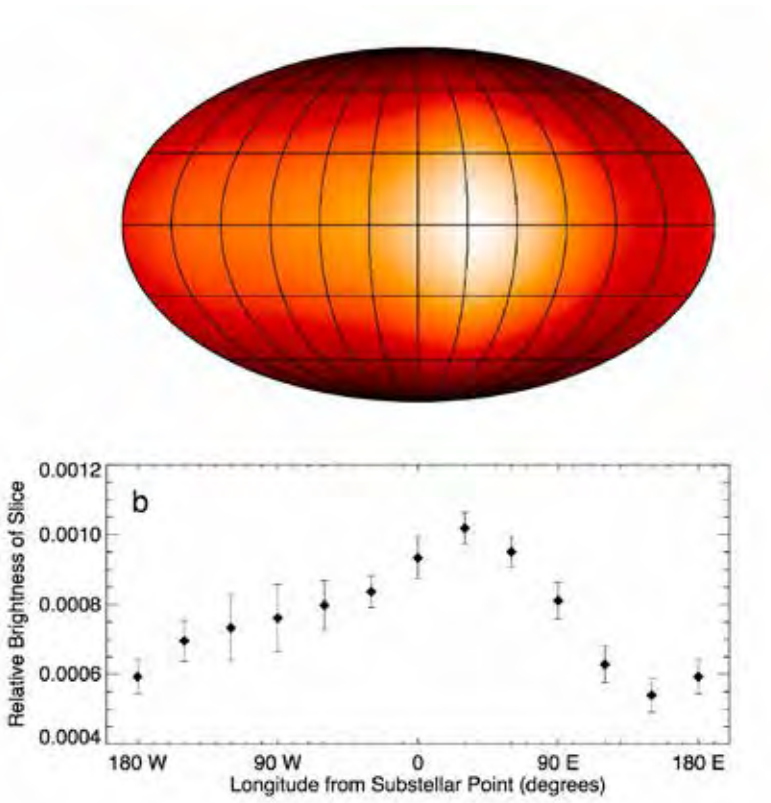

Linear, analytic solution for parameters relevant to hot, tidally locked exoplanets (Showman & Polvani 2011)

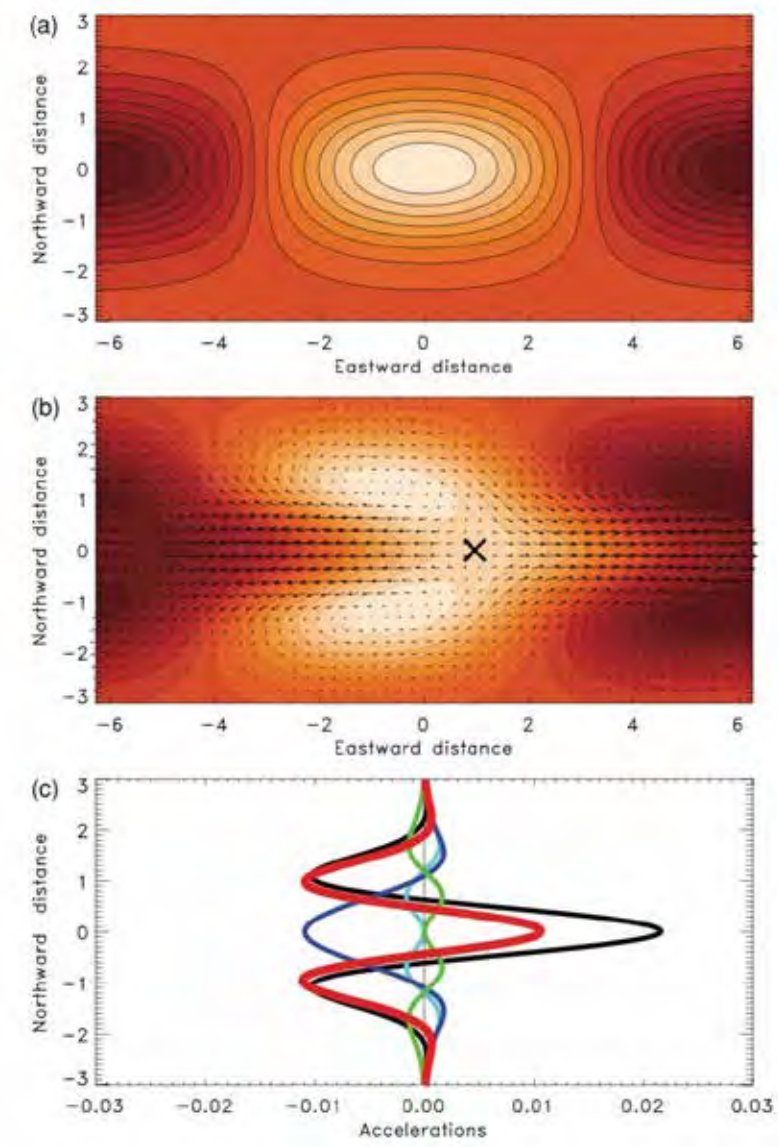

radiative-equilibrium height field

Height field (orange scale) and horizontal wind velocities (arrows)

Acceleration

Matsuno-Gill pattern (Matsuno 1966; Gill 1980)

- Heat-induced tropical circulation composed of Rossby wave and Kelvin wave
- Plays crucial roles in Earth's troposphere

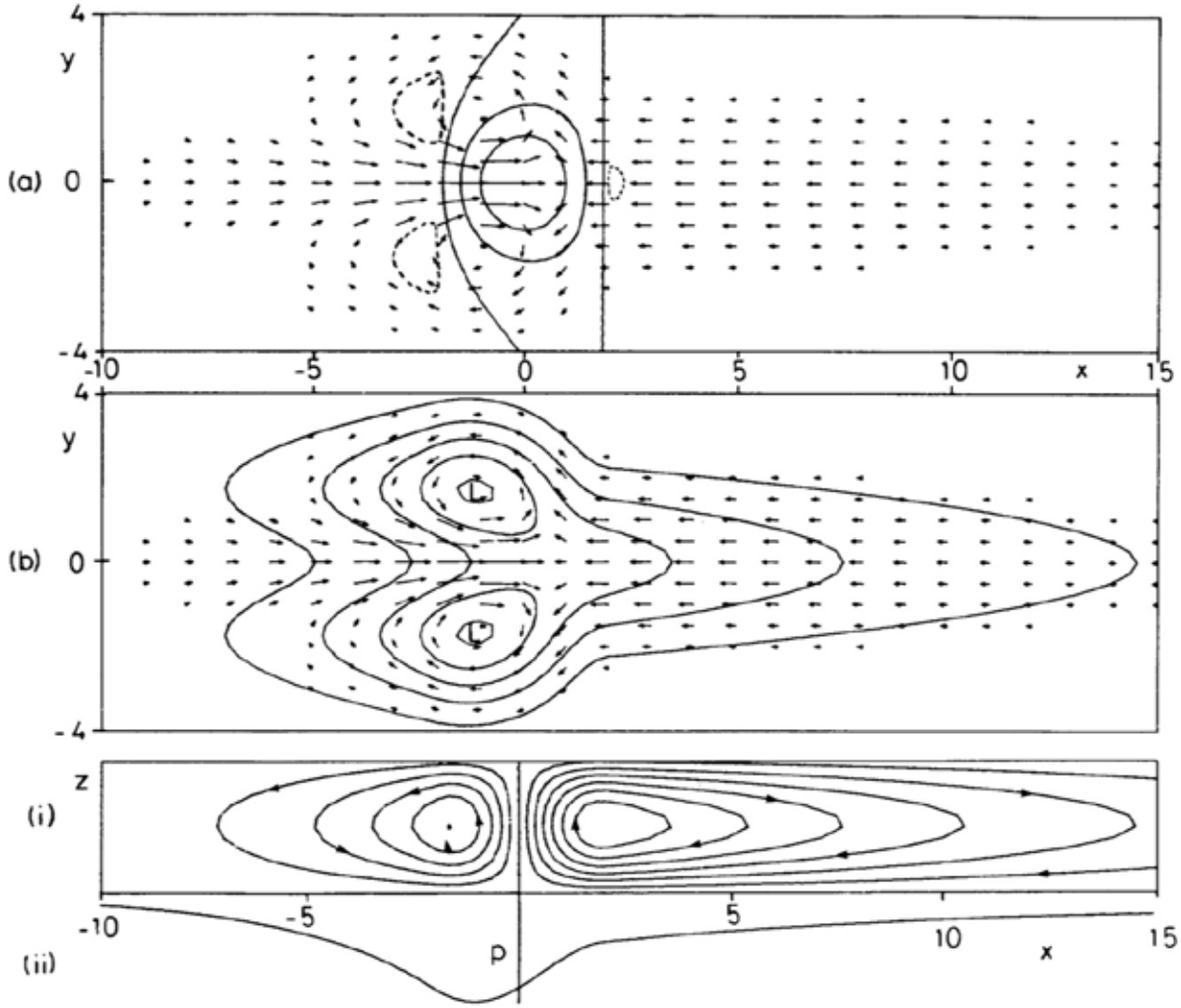

Figure 1. Solution for heating symmetric about the equator in the region $|x| < 2$ for decay factor $\varepsilon = 0{\cdot}1$.
(a) Contours of vertical velocity w (solid contours are 0, 0·3, 0·6, broken contour is −0·1) superimposed on the velocity field for the lower layer. The field is dominated by the upward motion in the heating region where it has approximately the same shape as the heating function. Elsewhere there is subsidence with the same pattern as the pressure field.

(b) Contours of perturbation pressure p (contour interval 0·3) which is everywhere negative. There is a trough at the equator in the easterly régime to the east of the forcing region. On the other hand, the pressure in the westerlies to the west of the forcing region, though depressed, is high relative to its value off the equator.
Two cyclones are found on the north-west and south-west flanks of the forcing region.

(c) The meridionally integrated flow showing (i) stream function contours, and (ii) perturbation pressure. Note the rising motion in the heating region (where there is a trough) and subsidence elsewhere. The circulation in the right-hand (Walker) cell is five times that in each of the Hadley cells shown in (c).

Driving forces of the zonally-averaged structure

Transformed Eulerian-mean equations:

Momentum eq.

$$\frac{\partial \bar{u}}{\partial t} + \bar{v}^* \left(\frac{\partial \bar{u}}{\partial y} - f \right) + \bar{w}^* \frac{\partial \bar{u}}{\partial z} = \frac{1}{\rho_0} \left(\frac{\partial F^{(y)}}{\partial y} + \frac{\partial F^{(z)}}{\partial z} \right)$$

zonal acceleration by waves

Residual mean meridional circulation
= Net Lagrangian transport

$$\bar{v}^* = \bar{v} - \frac{1}{\rho_0} \frac{\partial}{\partial z} \left(\rho_0 \frac{\overline{v'\theta'}}{\bar{\theta}_z} \right)$$

$$\bar{w}^* = \bar{w} + \frac{1}{\rho_0} \frac{\partial}{\partial y} \left(\frac{\overline{v'\theta'}}{\bar{\theta}_z} \right)$$

Eliassen-Palm flux (EP flux)

$$F^{(y)} = -\rho_0 \overline{u'v'}$$

$$F^{(z)} = -\rho_0 \left(\overline{u'w'} - f \frac{\overline{v'\theta'}}{\bar{\theta}_z} \right)$$

Thermal energy eq.

$$\frac{\partial \bar{\theta}}{\partial t} + \bar{v}^* \frac{\partial \bar{\theta}}{\partial y} + \bar{w}^* \frac{\partial \bar{\theta}}{\partial z} = \bar{Q}$$

diabatic heating

木田秀次(1983)

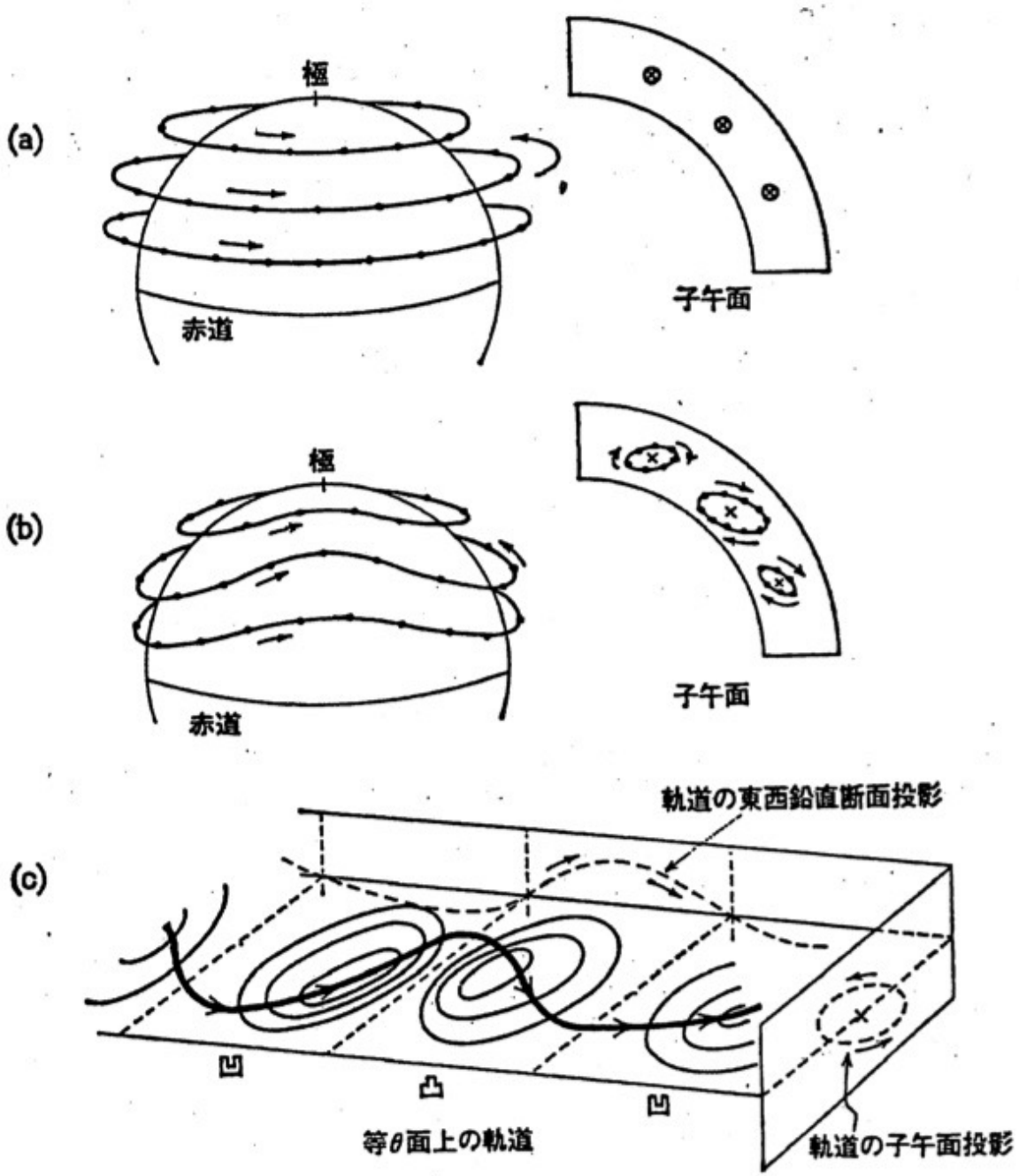

図 5.6 偏西風の中をプラネタリー波が鉛直伝播するときの空気塊の振動．小さい黒点は，微小空気塊を表わす．(a) 波が不在の場合．(b) 波が在る場合．× 印は子午面断面上の元の位置．(c) 等温位面上の空気塊の軌道．子午面投影では主軸が傾斜した楕円軌道になる．

Wave-driven meridional circulation

$$\cancel{\frac{\partial \bar{u}}{\partial t}} + \bar{v}^* \left(\cancel{\frac{\partial \bar{u}}{\partial y}} - f \right) + \bar{w}^* \cancel{\frac{\partial \bar{u}}{\partial z}} = \boxed{\frac{1}{\rho_0} \left(\frac{\partial F^{(y)}}{\partial y} + \frac{\partial F^{(z)}}{\partial z} \right)}$$

wave forcing

$$\therefore f\bar{v}^* = \boxed{\frac{1}{\rho_0} \left(\frac{\partial F^{(y)}}{\partial y} + \frac{\partial F^{(z)}}{\partial z} \right)}$$

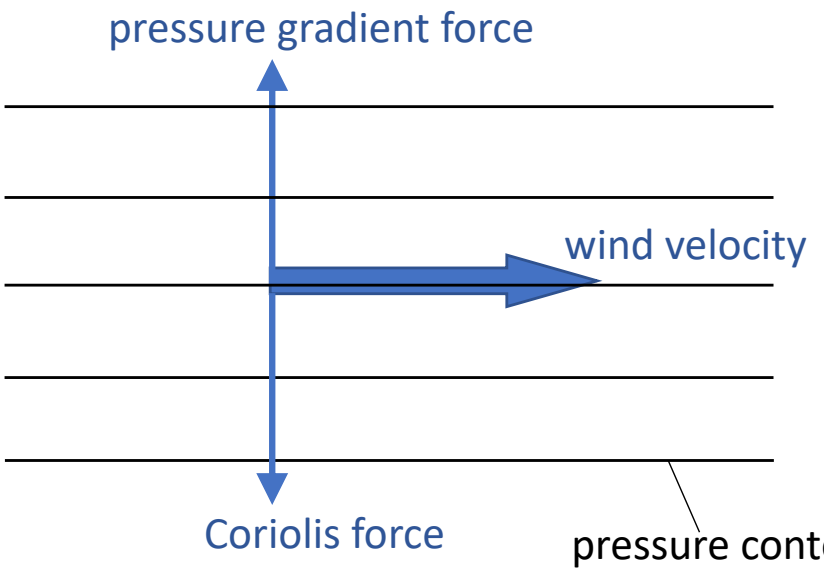

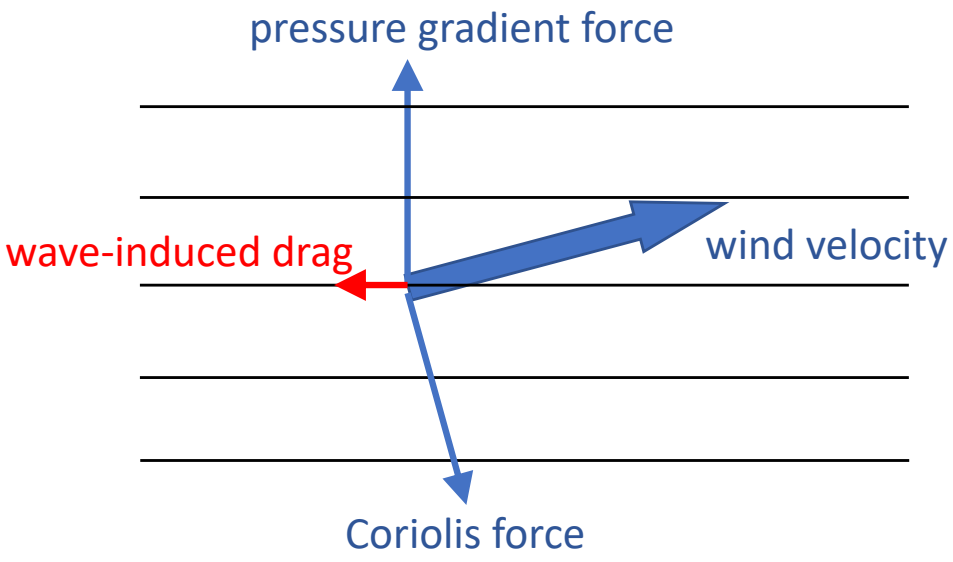

Earth's stratospheric meridional circulation (Holton 2012)

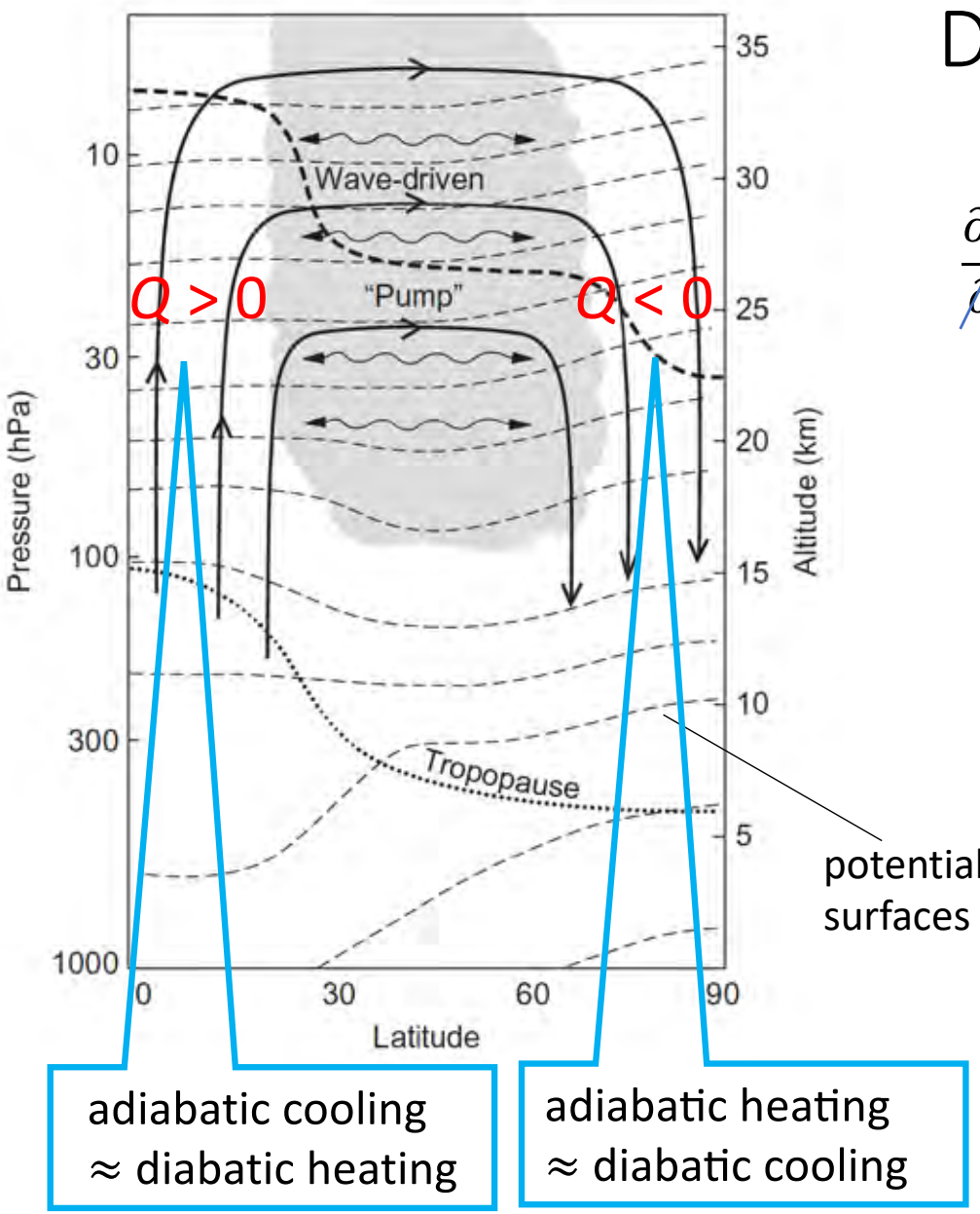

Diabatic circulation

$$\frac{\partial \bar{\theta}}{\partial t} + \bar{v}^* \frac{\partial \bar{\theta}}{\partial y} + \bar{w}^* \frac{\partial \bar{\theta}}{\partial z} = \bar{Q}$$

$$\bar{w}^* \frac{\partial \bar{\theta}}{\partial z} = \bar{Q}$$

adiabatic heating/cooling
断熱加熱

diabatic heating/cooling
非断熱加熱

Earth's mean meridional circulation in the troposphere

Holton 2004

Eulerian-mean

$(\bar{v}, \bar{w})$

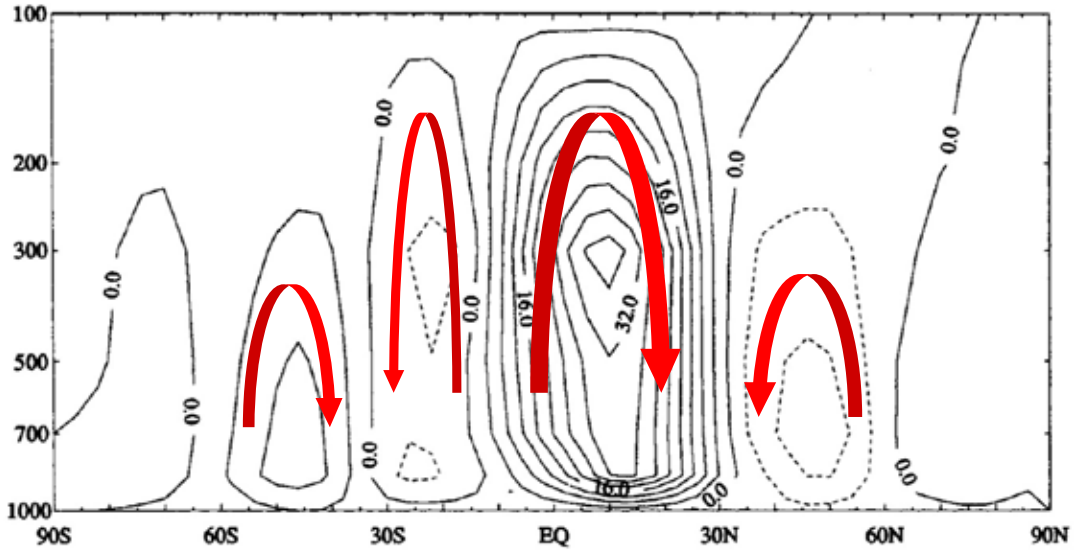

Fig. 10.7 Streamfunction (units: 10^2 kg m^{-1}s^{-1}) for the observed Eulerian mean meridional circulation for Northern Hemisphere winter, based on the data of Schubert et al. (1990).

Lagrangian-mean

$(\bar{v}^*, \bar{w}^*)$

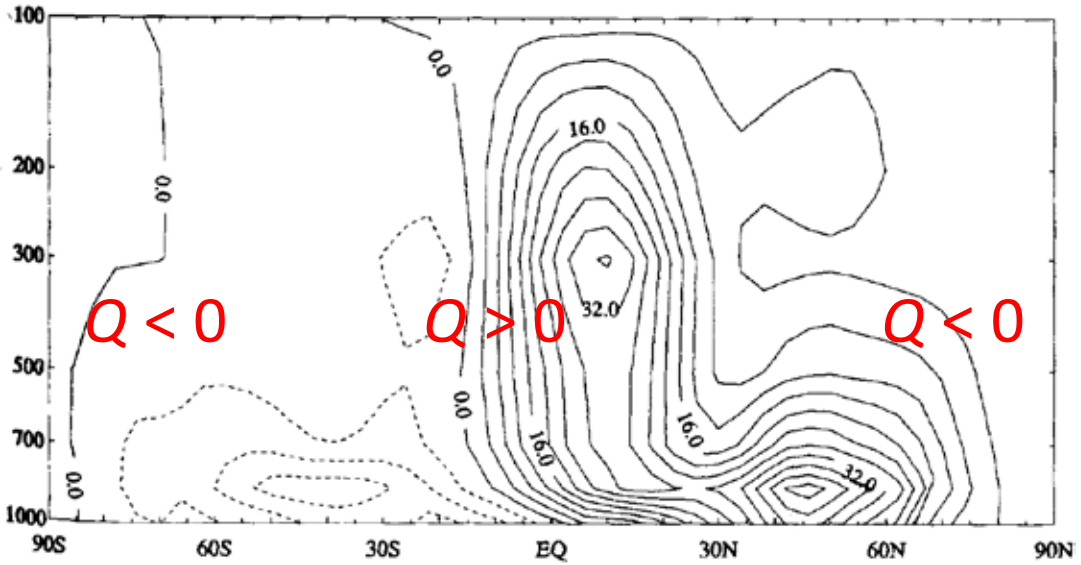

Meridional circulation of Mars atmosphere (Santee & Crisp 1995)

Mean temperature

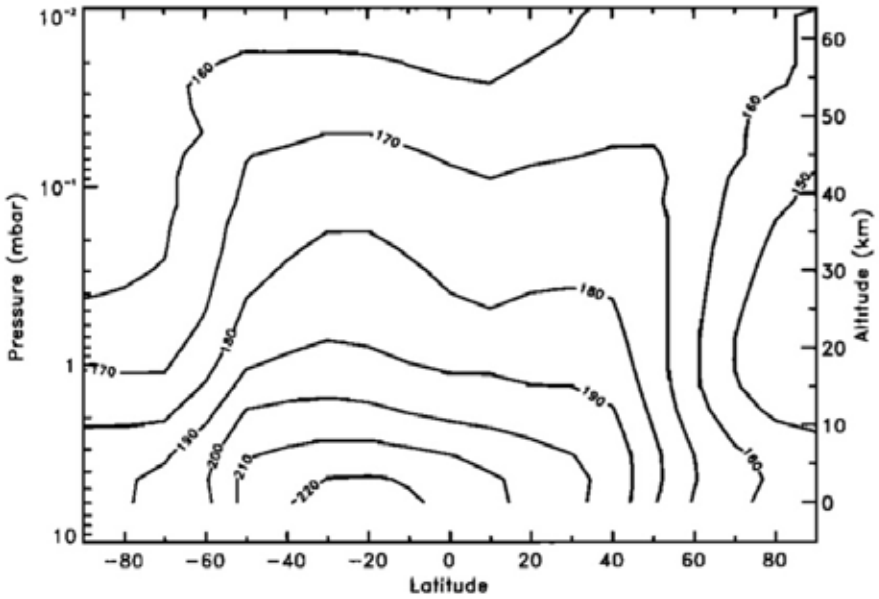

Figure 1a. Diurnal–mean temperatures obtained by averaging the 1400 LT and 0200 LT temperature maps retrieved from the Mariner 9 IRIS spectra in Paper I. For consistency with the results of Paper I, the vertical coordinate in this and all subsequent figures is the atmospheric pressure p. The approximate altitude z corresponding to a given pressure level is also included in these figures (see section 2.1). This correlation of altitude with pressure is based on the following values: $p_s = 6.0$ mbar, $R = 191.0$ J K^{-1} kg^{-1}, $g = 3.74$ m/s^2, and $T_0 = 196$ K (the globally and diurnally averaged value of the atmospheric temperature at the surface), resulting in a mean scale height $H = 10$ km.

Net radiative heating rate, Q

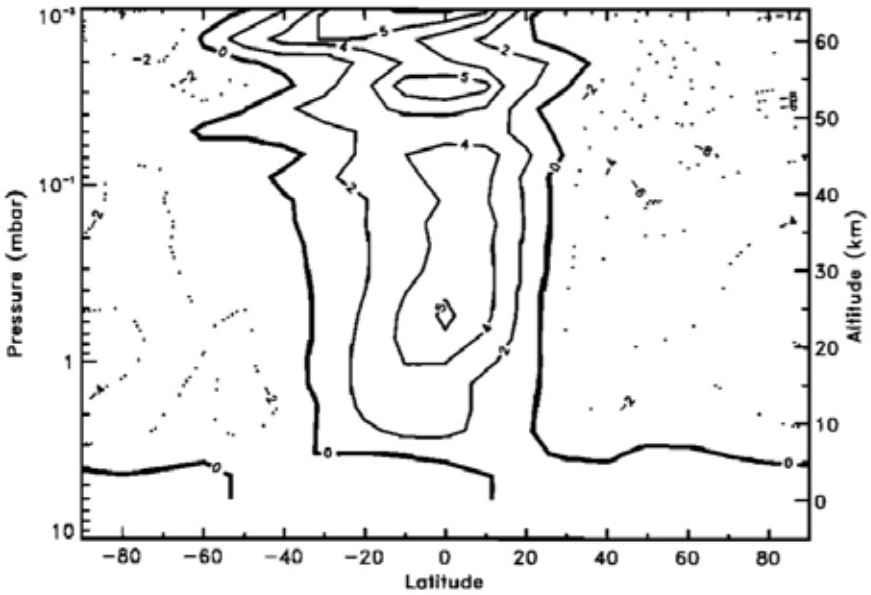

Figure 3. Net radiative heating rates (K/d) calculated from retrieved IRIS temperatures and dust abundances using the radiative transfer model described by *Crisp* [1990] and in the appendix of *Santee* [1993]. Negative contours are dashed, the zero contour is thicker, and the contour interval is nonuniform.

Meridional circulation of Mars atmosphere (Santee & Crisp 1995)

Meridional velocity $(\bar{v}^*)$

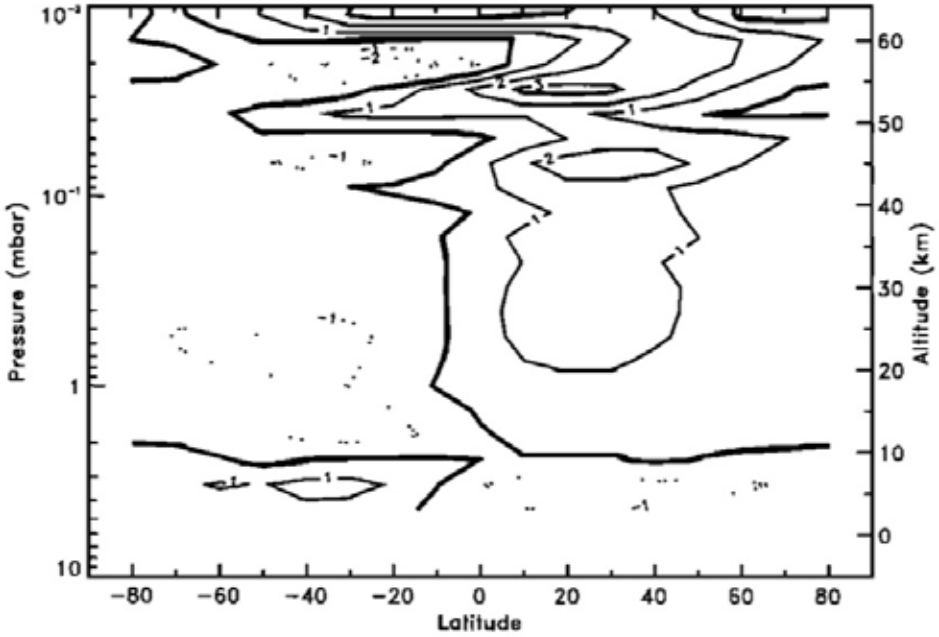

Figure 4a. Diabatic meridional velocity, in m/s. Positive values represent northward winds, negative contours are dashed, and the zero contour is thicker.

Vertical velocity $(\bar{w}^*)$

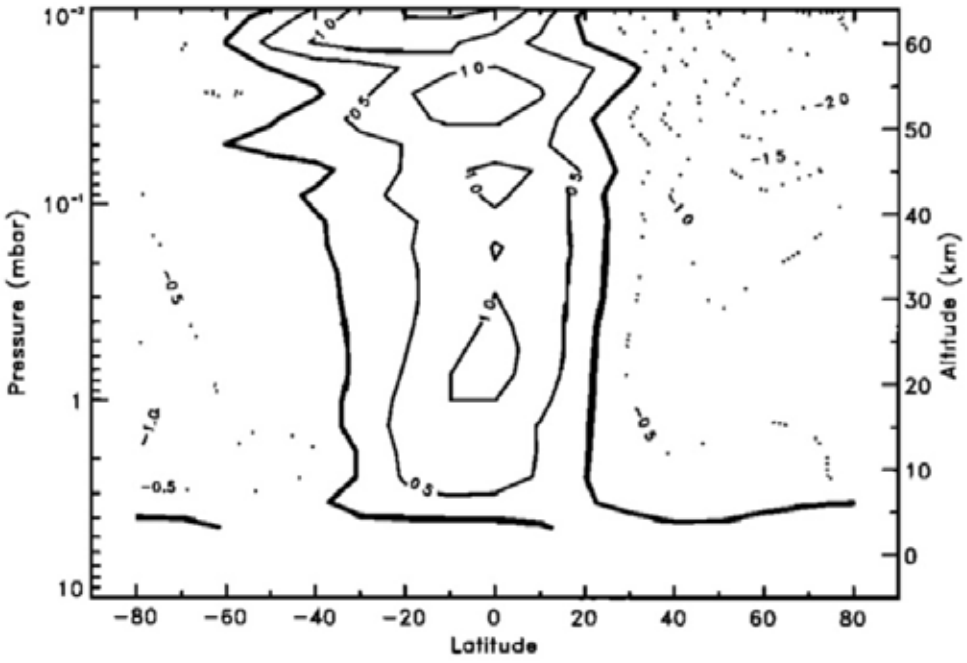

Figure 4b. Diabatic vertical velocity, in cm/s. Positive values represent upward winds, negative contours are dashed, and the zero contour is thicker.

Meridional circulation of Mars atmosphere (Santee & Crisp 1995)

Stream function

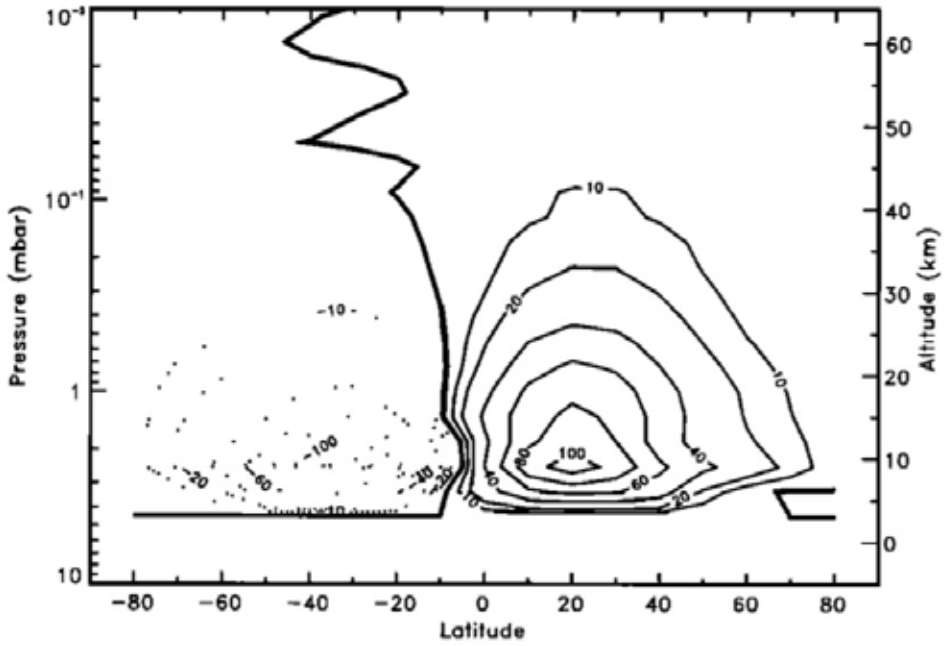

Figure 4c. Mass–weighted stream function, Ψ_m, in units of 10^7 kg/s. Positive values represent clockwise flow, negative contours are dashed, the zero contour is thicker, and the contour interval is nonuniform.

E-P flux divergence (zonal acceleration)

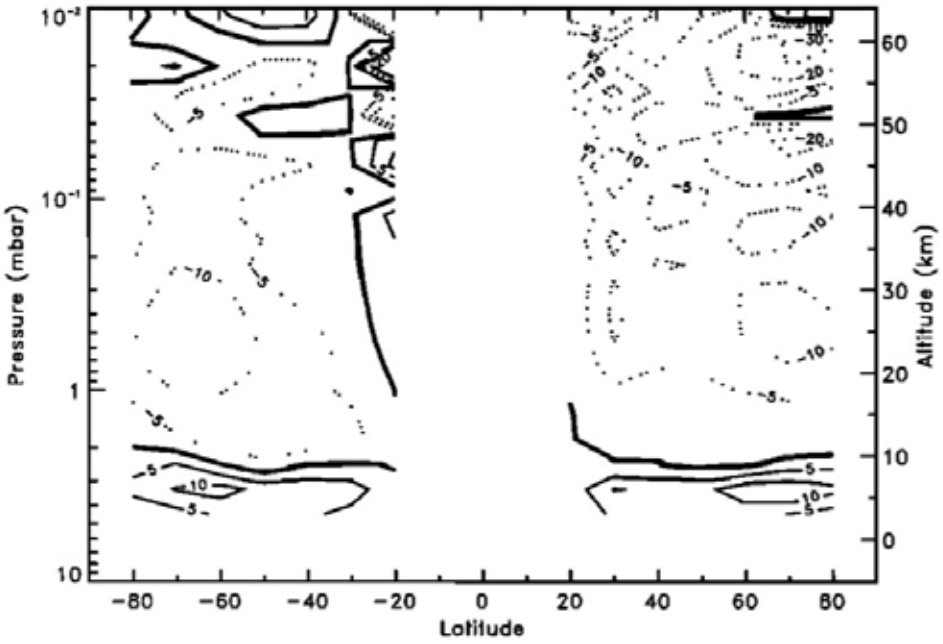

Figure 5. Eliassen–Palm flux divergence $((\rho a \cos\phi)^{-1} \nabla \cdot \mathcal{F})$ in units of $\mathrm{ms}^{-1}/\mathrm{d}$. Negative contours are dashed, the zero contour is thicker, and the contour interval is nonuniform.

temperature field

Meridional circulation of Venus atmosphere

Lee et al. (2015)

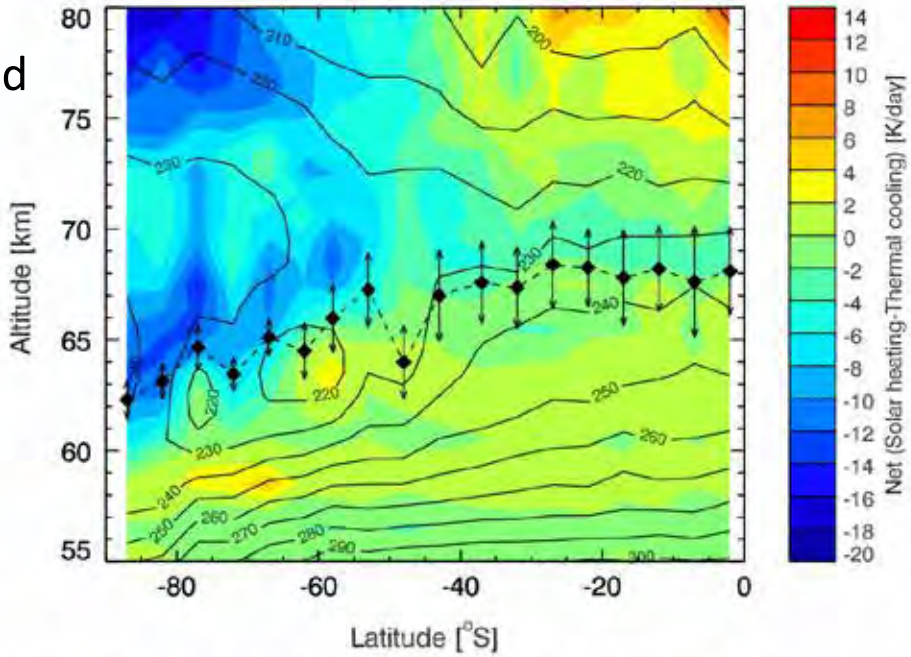

Fig. 14. Latitude–altitude field of the net radiative forcing in the Venus mesosphere. The temperature and cloud top structure are the same as in Figs. 9 and 13.

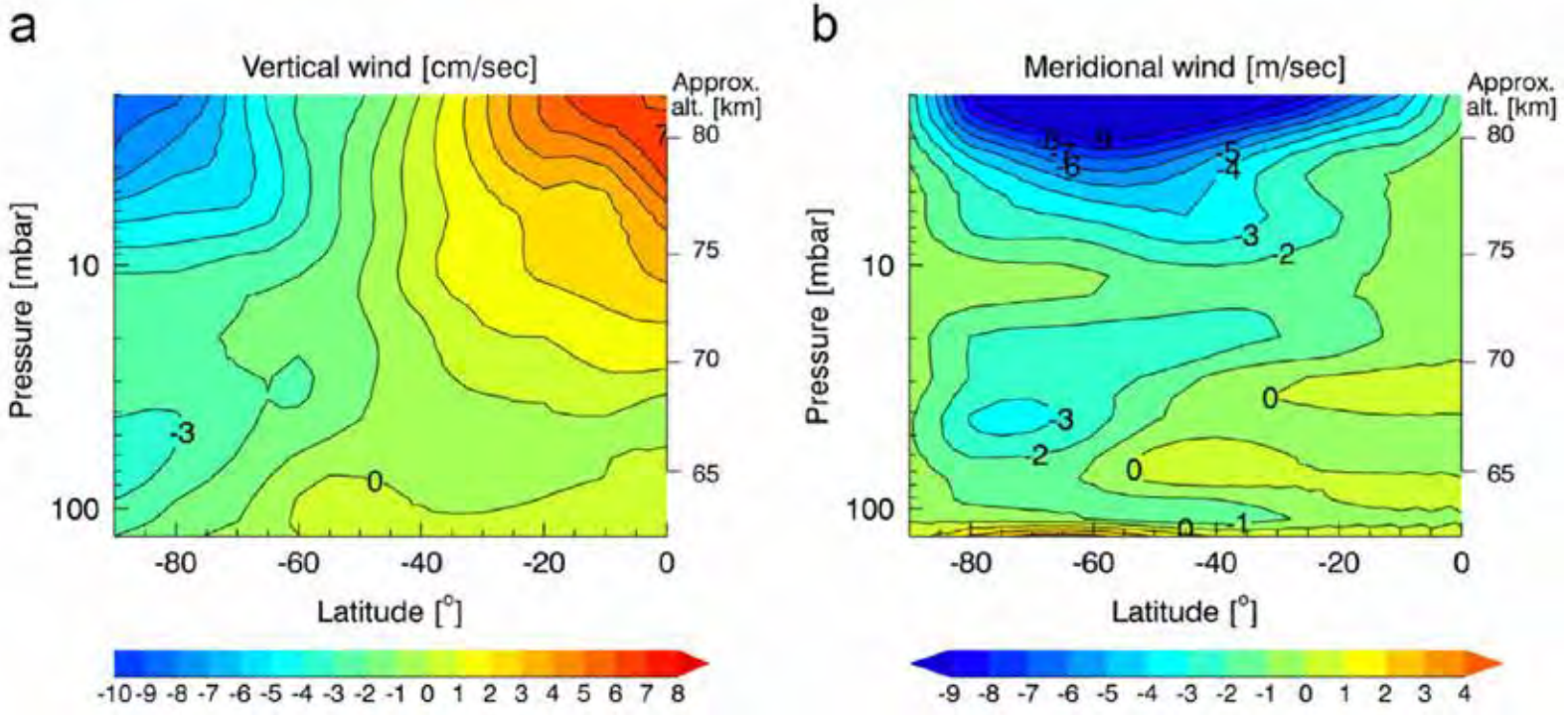

Hot polar dipole & cold collar at Venus's cloud top

Pioneer Venus thermal infrared mapping of the North polar region (Taylor et al. 1980)

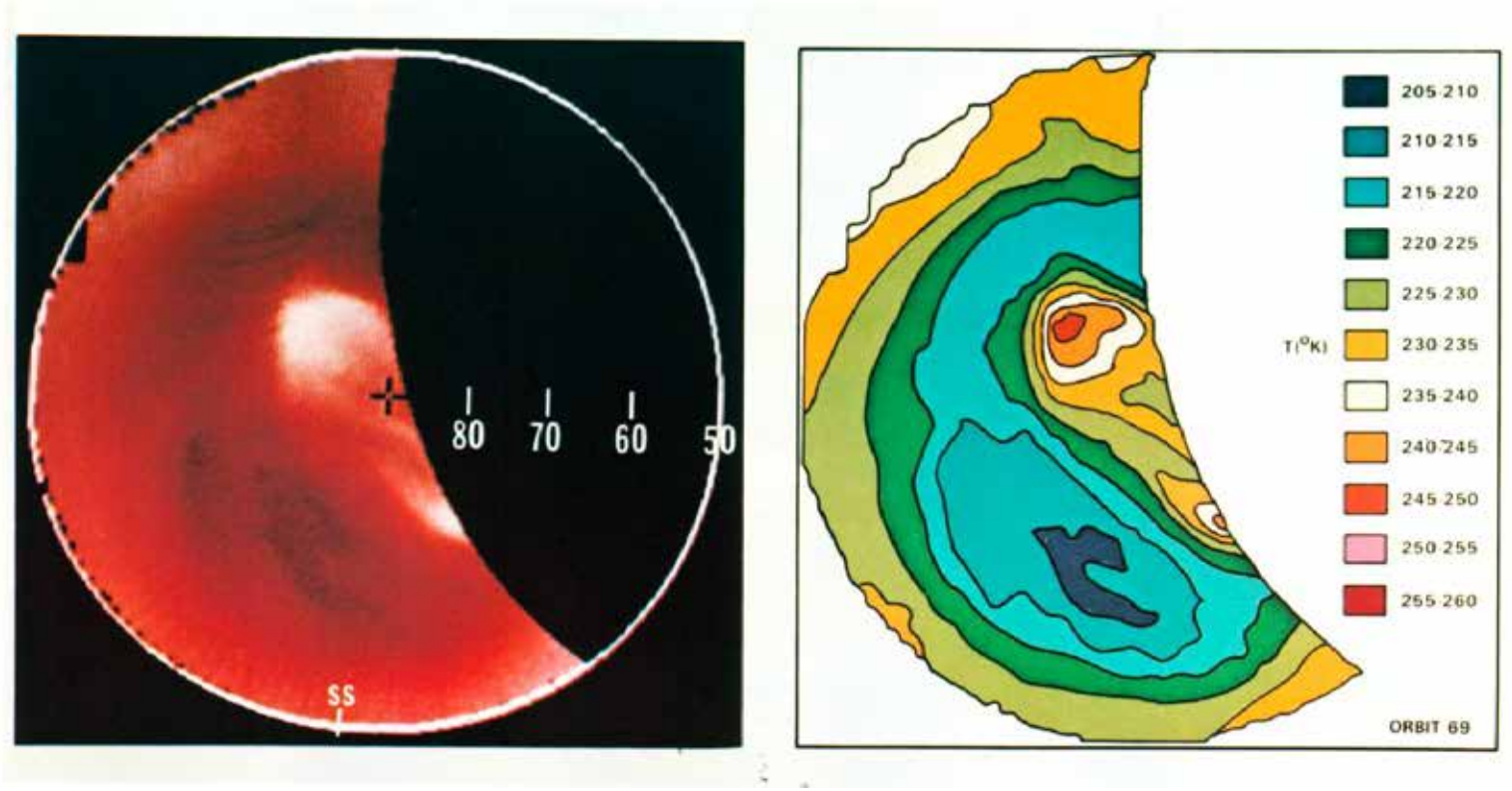

Ando et al. (2016)

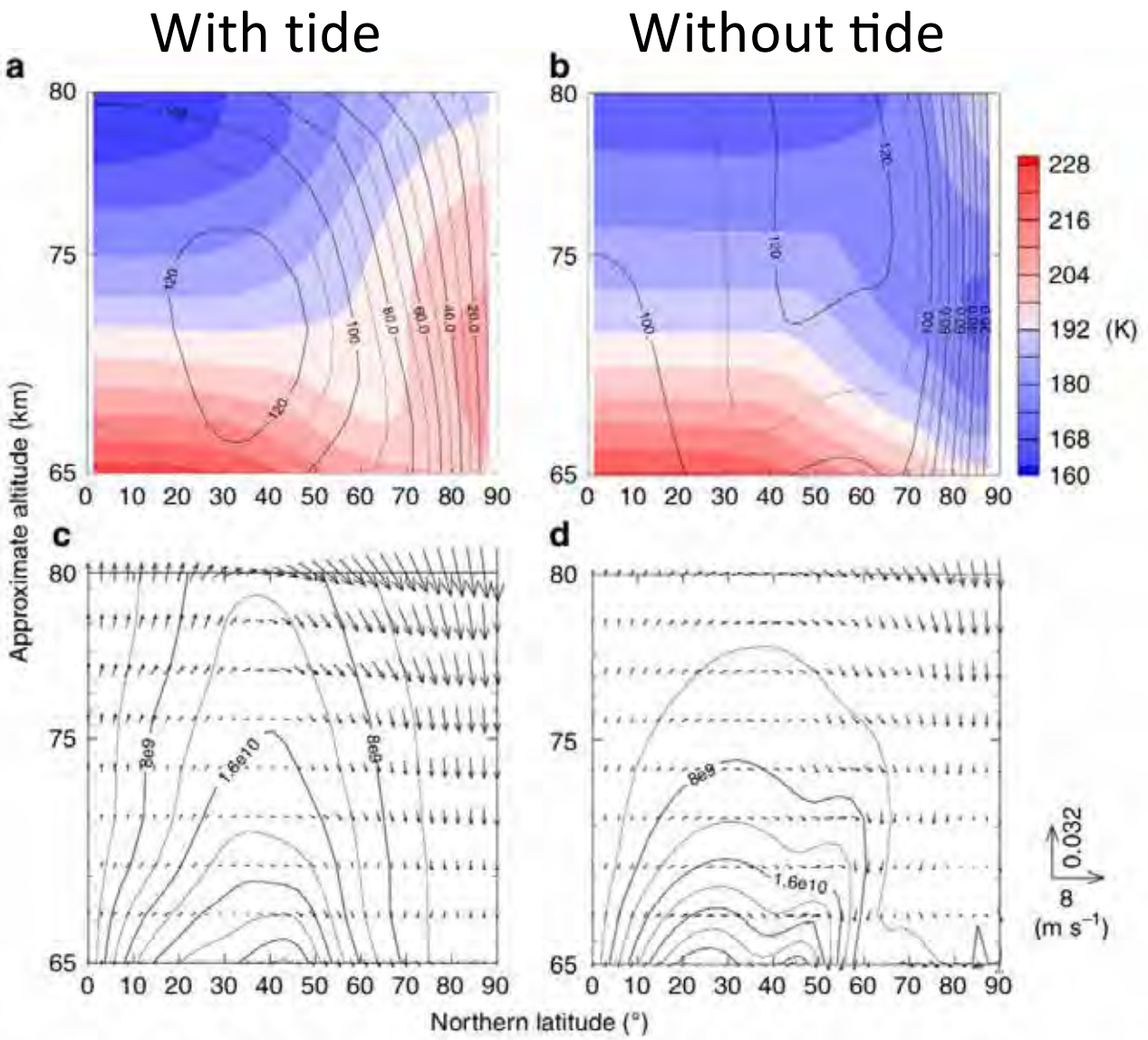

Figure 6 | Meridional cross-sections of the zonally and temporally averaged zonal wind (solid line) and temperature (colour shade) and the horizontal and vertical components of the residual mean meridional circulation (vector) and mass stream fuction (contour). (**a**) Zonal wind and temperature in Case A. (**b**) Those in Case B. (**c**) Residual mean meridonal circulation vector and mass stream function in Case A. (**d**) Those in Case B. Averaged period is two Venusian solar days (234 Earth days) after settling into the quasi-steady state.